A new early water frog (Telmatobius) from the Miocene of the Bolivian Altiplano

Raúl Gómez, Tomás Ventura, Guillermo Turazzini, Laurent Marivaux, Rubén Andrade Flores, Alberto Boscaini, Marcos Fernández-Monescillo, Bernardino Mamani Quispe, Mercedes Prámparo, Séverine Fauquette, et al.

Papers in Palaeontology (https://doi.org/10.1002/spp2.1543)

A new early water frog (*Telmatobius*) from the Miocene of the Bolivian Altiplano

by RAÚL O. GÓMEZ[1,2]*, TOMÁS VENTURA[1], GUILLERMO F. TURAZZINI[1,2], LAURENT MARIVAUX[3], RUBÉN ANDRADE FLORES[4], ALBERTO BOSCAINI[5,2], MARCOS FERNÁNDEZ-MONESCILLO[6,2], BERNARDINO MAMANI QUISPE[4], MERCEDES B. PRÁMPARO[7,2], SÉVERINE FAUQUETTE[3], CÉLINE MARTIN[8], PHILIPPE MÜNCH[8], FRANÇOIS PUJOS[7,2] *and* PIERRE-OLIVIER ANTOINE[3]*

[1] Departamento de Biodiversidad y Biología Experimental, Facultad de Ciencias Exactas y Naturales, Universidad de Buenos Aires, Ciudad Universitaria, C1428EGA Buenos Aires, Argentina; raulorenciogomez@gmail.com; 0000-0002-6600-3787 (Raúl O. Gómez); 0000- 0003-4284-5178 (Guillermo F. Turazzini)

[2] Consejo Nacional de Investigaciones Científicas y Técnicas (CONICET), Godoy Cruz 2290, C1425FQB Buenos Aires, Argentina

[3] Institut des Sciences de l'Évolution de Montpellier, Univ. Montpellier, CNRS, IRD, F-34095 Montpellier, France; pierre-olivier.antoine@umontpellier.fr; 0000-0002-2882-0874 (Laurent Marivaux); 0000-0003-0516-7734 (Séverine Fauquette); 0000-0001-9122-1818 (Pierre-Olivier Antoine)

[4] Unidad de Paleontología, Museo Nacional de Historia Natural, Calle 26 s/n, Cota Cota, La Paz, Plurinational State of Bolivia

[5] Instituto de Ecología, Genética y Evolución de Buenos Aires (IEGEBA), Facultad de Ciencias Exactas y Naturales, Universidad de Buenos Aires, Ciudad Universitaria, C1428EGA Buenos Aires, Argentina; 0000-0002-8666-9340 (Alberto Boscaini)

[6] Cátedra y Museo de Paleontología, Facultad de Ciencias Exactas, Físicas y Naturales, Universidad Nacional de Córdoba. Vélez Sarsfield 1611, X5016GCA Córdoba, Argentina; 0000-0002-0698-1909 (Marcos Fernández-Monescillo)

[7] Instituto Argentino de Nivología Glaciología y Ciencias Ambientales (IANIGLA), CONICET-UNCUYO-Mendoza, Avda. Ruiz Leal s/n, Parque Gral. San Martín, 5500 Mendoza, Argentina; 0000-0002-3955-8496 (Mercedes B. Prámparo); 0000-0002-6267-3927 (François Pujos)

[8] Géosciences Montpellier, Univ. Montpellier, CNRS, Université des Antilles, F-34095 Montpellier, France; 0000-0003-4616-8039 (Philippe Münch)

*Corresponding authors

Abstract: We describe the new frog *Telmatobius achachila* sp. nov. from the late Middle–earliest Late Miocene of Achiri, based on a partial skeleton found at 3960 m above sea level in the Bolivian Altiplano. This skeleton, attributed to an adult male, constitutes the first documented fossil record of the speciose living genus *Telmatobius*, endemic to the Andean Cordillera and the Altiplano. Phylogenetic analyses confirm the new species as being part of the crown group, and diverging both later than the *T. verrucosus* group and earlier than the *T. bolivianus*, *T. marmoratus*, and *T. macrostomus* groups. Coupled with its accurate stratigraphic provenance and age, such phylogenetic position provides a relevant calibration point for timing the evolutionary history of these highland, mostly aquatic frogs. The skeleton of *T. achachila* indicates that several of the osteological peculiarities of extant *Telmatobius* were already acquired *c*. 12 Ma ago, including some that might be linked to their aquatic lifestyle. Together with mixed montane-rainforest pollen vegetation uncovered in the same level, this fossil specimen further provides key data allowing for a more accurate reconstruction of ancestral habitats and elevation ranges of *Telmatobius*, agreeing with the previously-postulated conditions in which these Water frogs might have first evolved. Ultimately, this discovery adds to the scarce evidence of a humid tropical Bolivian Altiplano just prior to i) the Late Miocene uplift pulse of the Central Altiplano and ii) the drastic climate deterioration that occurred in Late Miocene times onward, leading to the harsh highland-steppe environments reigning there today.

Key words: Achiri, Altiplano, calibration point, frog, Miocene, *Telmatobius*

INTRODUCTION

FROGS of the genus *Telmatobius* Wiegmann, 1834 constitute the most diverse group of anurans in the Andean highlands, with 61 extant species in the genus (Frost 2023) ranging from roughly the equator in the north to nearly 30°S in Argentina (Cei 1986; De la Riva *et al.* 2010; Barrionuevo 2017). Most species inhabit high altitudes in the Andes, surpassing 3000 m above sea level (ASL) and up to 5244 m (De la Riva 2005; Lavilla & Barrionuevo 2005; Seimon *et al.* 2007), whereas only a dozen of species can be found today at average elevations between 1500 and 2500 m ASL (Wiens 1993; De la Riva & Harvey 2003; De la Riva *et al.* 2012). The genus name *Telmatobius*, as their common name (Water frogs), alludes to their mostly aquatic habits in a variety of environments, including mountain streams of temperate humid realms such as cloud forests, as well as streams, ponds, peat bogs, thermal springs, and lakes of the colder and drier highlands of the Altiplano and Puna (Vellard 1951; De la Riva 2005; Barrionuevo 2017). The aquatic highland species adapted to the harsh conditions of highland environments (Vellard 1951; Sáez *et al.* 2022), such as the endangered Titicaca Water Frog (*Telmatobius culeus*; IUCN SSC Amphibian Specialist Group 2020), show morphological, physiological, and ecological peculiarities related to feeding and communicating underwater (Barrionuevo 2016; Brunetti *et al.* 2017; Muñoz-Saravia 2018), as well as to enduring low oxygen levels and pronounced temperature fluctuations (Hutchison *et al.* 1976; Weber 2014; Muñoz-Saravia *et al.* 2018).

The mode of life of these frogs under extreme environmental conditions would have shaped their relatively conserved external phenotype (Vellard 1951; De la Riva 2005; Sáez *et al.* 2022), which, coupled with the low genetic divergence shown by some highland clades (De la Riva *et al.* 2010; Sáez *et al.* 2014, 2022), suggest that most lineages within *Telmatobius* diversified quite recently, during Pliocene times (i.e. less than 5 million years ago; De la Riva *et al.* 2010). This has made it difficult to resolve their evolutionary relationships based on external morphology or molecular data alone (De la Riva *et al.* 2012; Barrionuevo 2017), yet the monophyly of *Telmatobius* is currently considered well supported (De la Riva *et al.* 2010; Sáez *et al.* 2014, 2022; Barrionuevo 2017), and includes species formerly assigned to *Batrachophrynus* (Aguilar & Valencia 2009; Frost 2023). In contrast to the pattern shown by soft anatomy and gene data, skeletal morphology in *Telmatobius* shows substantial interspecific variation (Trueb 1979; Wiens 1993; De la Riva *et al.* 2012; Barrionuevo 2018), although intraspecific variation in some osteological features has also

been described (e.g. Sinsch *et al.* 2005; Barrionuevo 2013). This substantial interspecific variation has led to reporting species' osteology (De la Riva *et al.* 2012) and to infer their phylogenetic relationships based on osteology (Barrionuevo 2017). Molecular (De la Riva *et al.* 2010; Sáez *et al.* 2014) and morphological (Aguilar & Valencia 2009; Barrionuevo 2017) phylogenetic cladistic analyses recovered four major clades within the genus: i) the *T. verrucosus* group, including mostly semiaquatic species from the cloud forests and adjacent humid paramos in Bolivia and Peru (De la Riva 2005; Aguilar *et al.* 2012); ii) the *T. bolivianus* group, with primarily aquatic forms inhabiting streams in mountain forests and other habitats at intermediate elevations in Bolivia and Argentina (De la Riva 2005; Lavilla & Barrionuevo 2005); iii) the *T. macrostomus* group, mostly aquatic species from the Andean highlands in Peru (Aguilar & Valencia 2009; Barrionuevo 2017); and iv) the *T. marmoratus* group, including the *T. hintoni* and *T. zapahuirensis* groups of Sáez *et al.* (2014), mainly consisting of aquatic species from the dry Altiplano-Puna highlands in Peru, Bolivia, Chile, and Argentina (De la Riva 2005; Lavilla & Barrionuevo 2005; Formas *et al.* 2006; Aguilar & Valencia 2009; Barrionuevo 2017).

Telmatobius has been hypothesised to have a forest origin in the Andean region, likely during the Miocene, with highland species in drier habitats having evolved more recently when the Andean uplift promoted isolation of different populations (Duellman 1979; Cei 1986; Lynch 1986; De la Riva *et al.* 2010). However, this hypothesis and the chronology and geography of the early diversification of *Telmatobius* remain highly speculative (De la Riva *et al.* 2010). This is due in part to the uncertain timing of the diversification of *Telmatobius* (De la Riva *et al.* 2010; Sáez *et al.* 2014), which, in turn, relates to the lack of reliable fossil calibration points (De la Riva *et al.* 2010). The fossil record of *Telmatobius* is almost null, as unfortunately observed for most anuran genera from the Neotropics (Gómez *et al.* 2013; Turazzini *et al.* 2014, 2016; Pérez-Ben *et al.* 2019; Barcelos & dos Santos 2022; Turazzini & Gómez 2023a), and restricted to so far undescribed isolated bones attributed to *Telmatobius* sp. that have recently been reported from the Pleistocene of Chile (Figueroa-Bravo *et al.* 2022).

Here we report on an outstanding record from the late Middle–earliest Late Miocene of Achiri, at 3960 m ASL in the Bolivian Altiplano (Fig. 1), which consists of several associated cranial and postcranial bones referable to a single adult male of a new species of *Telmatobius*. We provide a detailed description of its cranium and postcranium and perform phylogenetic analyses that confirm the new species as part of the crown group *Telmatobius*.

We also perform stochastic character mapping to reconstruct the ancestral substrate preference, habitat, and elevation range of *Telmatobius*, highlighting the impact of the new species in inferring the palaeoecology and palaeobiogeography of the group. Finally, we discuss the potential of the new record as a reliable calibration point for timing the evolutionary history of this speciose group of Andean frogs.

GEOLOGICAL SETTING

A few Miocene fossil-bearing loci (levels + localities) have been described near the Achiri village (e.g. Saint-André 1993; Pujos *et al.* 2012; Fernández-Monescillo *et al.* 2019; Gaudin *et al.* 2022; Prámparo *et al.* 2022 and references therein; Fig. 1A). All of them were deposited in a vast fluvial and lacustrine plain, and are assigned to the uppermost member (Member 6 or M6) of the volcaniclastic-dominated Mauri Formation (Sirvas-Carranza and Torres 1966; Saint-André 1993). Classical mammal-yielding levels of the M6, first described half a century ago (Hoffstetter *et al.* 1972; Villarroel 1974), correlate with the mammal-bearing locus (level + site) ACH-27 located *c.* 80 m above the base of the Cerro Pisakeri (Fig. 1A) and bracketed by volcanic ashes dated by one of us (PM) at 10.42 ± 0.09 Ma and 9.42 ± 0.1 Ma (Late Miocene; Fernández-Monescillo *et al.* 2019; Gaudin *et al.* 2022; Prámparo *et al.* 2022; Fig. 1B). Over the last decade, our team discovered older fossil-bearing levels within M6 at different sites (loci) at the bottom of the available Cerro Pisakeri stratigraphic section (Prámparo *et al.* 2022; Fig. 1B). These fine-grained and plant-rich green marls are indicative of lacustrine and low-energy fluvial settings in the area, which is confirmed by the palynological assemblage recovered at the loci ACH-25 and ACH-26 (Prámparo *et al.* 2022). The *Telmatobius*-yielding locus ACH-14 is a white, tuffaceous, fine-grained laminated siltite of low-energy fluviolacustrine origin, intercalated between green marl-dominated beds that crops out 4 km south of Achiri near the base of Cerro Pisakeri (Prámparo *et al.* 2022; Fig. 1). A thorough stratigraphical survey in May 2022 indicated this 50 cm-thick tuffaceous siltite is laterally equivalent to locus ACH-26 in the section (Fig. 1B), instead of being located 3 m above of it as previously illustrated in Prámparo *et al.* (2022). Accordingly, a late Middle to early Late Miocene age can be hypothesised for ACH-14 (see discussion in Prámparo *et al.* 2022).

MATERIAL AND METHOD

The holotype specimen in block MNHN-Bol-V 012795, upon which we erect a new extinct species of *Telmatobius*, was collected in situ by three of us (POA, BMQ, and RAF) during an expedition in the Bolivian Altiplano at Achiri, in 2011. It is permanently curated in the fossil vertebrate collections of the Museo Nacional de Historia Natural de Bolivia at La Paz (MNHN-Bol-V). Other fossils were collected in the same field campaign, as well as in 2015 and 2022, by members of the same team (POA, RAF, LM, FP, and SF). All fossil specimens (holotype of the new *Telmatobius* species and other microvertebrate materials) come from the locus ACH-14, from a single lamina of fine-grained tuffaceous siltite of lacustrine origin. The holotype skeleton was collected in the same block with a few remains of a much smaller but putatively-conspecific frog, the remains of which are too fragmentary and do not add meaningful data, and a bird, which will be described elsewhere. Several of these bones have already been mechanically isolated from the matrix, but a few ones belonging to the holotype of the new frog species are still associated in the main block (Figs. 2A, S1). Most of the skeletal elements of the holotype are three-dimensional bones that are preserved as disarticulated but closely associated. Their relative size, number, and morphology strongly indicate that they all belonged to a single adult male frog (Figs. 2B, S1).

For comparisons, we surveyed skeletons of most hyloid families, but also pipids and microhylids, with a focus on *Telmatobius* and other hyloids currently considered phylogenetically related, primarily relying on direct examination of dry skeletons, cleared-and-stained specimens, and three-dimensional (3D) models from CT-data available at MorphoSource (https://www.morphosource.org), but also on published data (see Appendix S1). The 3D models were generated following the workflow of Buser *et al.* (2020), using Fiji (ImageJ v.1.53c; Schindelin *et al.* 2012) and 3D Slicer v.4.11.2 (Fedorov *et al.* 2012; Kikinis *et al.* 2014). Measurements of limb bones were those defined by Lires *et al.* (2016), but also including the length of metacarpal IV and considering epiphyses. Measurements were taken digitally either on Fiji (from photographs) or 3D Slicer (from 3D models). General anatomical terminology follows Gaupp (1896), Bolkay (1919), Maglia *et al.* (2007), and Turazzini & Gómez (2023b), with most Latin terms translated into English. Carpal terminology follows Gaupp (1896), Fabrezi (1992), and Fabrezi & Alberch (1996), and pelvic terminology follows Gómez & Turazzini (2016). The orientation of limbs follows Gaupp (1896). The general

taxonomic scheme for anurans follows Frost (2023) and the systematic arrangement of *Telmatobius* follows De la Riva *et al.* (2010) and Barrionuevo (2017).

Phylogenetic analyses

In order to test the evolutionary relationships of the new fossil frog from Achiri, quantitative phylogenetic analyses were performed, incorporating data from MNHN-Bol-V 012795 in the available data matrix of Barrionuevo (2017; hereafter referred as dataset B17) and a taxonomically reduced version of the matrix from Gómez & Turazzini (2021a; hereafter referred to as dataset GT21). The matrix of Barrionuevo (2017; permalink https://morphobank.org/permalink/?P2723) was initially designed for testing the monophyly of *Telmatobius* and their internal relationships, including 97 morphological characters (two continuous; 59 of the adult skeleton) scored for 43 species of *Telmatobius* plus 13 outgroup taxa from five families. This dataset therefore met our purposes of testing the presumed affinities of the new extinct species of *Telmatobius*, yet the osteological character sampling is rather poor. The matrix of Gómez & Turazzini (2021b; permalink https://morphobank.org/permalink/?P4531), originally designed for testing the relationships of extinct and extant Ceratophryidae, included among the outgroup six species of *Telmatobius* representing several major lineages within the genus plus 15 additional non-ceratophryid taxa and 256 discrete characters of the adult skeleton, thereby representing a rigorous test of higher level relationships and a potential source of additional apomorphies. We deleted nearly all ceratophryids from this latter dataset, keeping one species of each extant genus, so the final dataset GT21 included a total of 18 non-telmatobiid extant taxa representing eight families, thus providing a broad overlap with the outgroup of dataset B17. The character scoring of the new fossil species is provided in Appendix S2.

Matrices were assembled in MESQUITE v3.6 (Maddison & Maddison 2018) and analysed in TNT v1.5 (Goloboff & Catalano 2016). Parsimony analyses were performed under both equal and implied weights (Goloboff 1993) across a range of mild concavity constant values (k = 5–9) and treating multistate characters in dataset B17 as either ordered or unordered, replicating previous settings (Barrionuevo 2017; Gómez & Turazzini 2021a). We performed heuristic searches using 'New Technologies' with sectorial searches, tree fusing, and ratchet, followed by tree bisection–reconnection (TBR) branch swapping to hit independently 10 times the optimal scoring and holding up to 100000 most parsimonious

trees (MPTs), plus a final round of TBR. In each case, basic statistics were performed (tree length; Consistency Index [CI]; Retention Index [RI]) and, when appropriate, a strict consensus of the MPTs was calculated to summarise the phylogenetic results. Node support was estimated in TNT v1.5 using the Bremer index (BS) and Jackknifing (JK); the latter was expressed as absolute frequencies calculated with 10000 pseudo-replicates of 10 random sequence additions each followed by TBR swapping, keeping up to 10 trees, with a probability of alteration P = 0.36.

Ancestral reconstructions of substrate preference, habitat, and elevation

We explored the congruence (and potential impact) of palaeoecological, palaeoenvironmental, and palaeoelevation data associated with the new frog from Achiri, as inferred from multiple proxies including stable isotopes, leaf physiognomy, palynology, and skeletal morphology (Garzione *et al.* 2017; Martínez *et al.* 2020; Prámparo *et al.* 2022; this paper), with ancestral reconstructions of substrate preference, habitat, and elevation in *Telmatobius* based exclusively on data from 43 of 61 extant species (see Appendix S3). Substrate preferences (terrestrial; semi-aquatic; aquatic), main habitats (forests; shrubland/grasslands; highland wetlands), and mean range elevation for extant species of *Telmatobius* were gathered from the IUCN Red List of Threatened Species (www.iucnredlist.org, accessed on 7 January 2023), augmented by information presented by De la Riva (2005) for Bolivian species. Mean range elevation was discretised into three range categories using *k*-means clustering performed in R v.3.6.3 (R Core Team 2013), resulting in ranges roughly equivalent to mid-low (1500–2500 m ASL), mid-high (2501–3500 m ASL), and high elevations (3501–4300 m ASL). Ancestral states were optimised on a time-adjusted optimal tree derived from the analysis under implied weights (k = 7) of the dataset B17, assembled in MESQUITE v3.6 (Maddison & Maddison 2018). Node ages, when available, were obtained directly from the Bayesian Markov Chain Monte Carlo estimates of De la Riva *et al.* (2010), under a medium-slow nucleotide substitution rate of 1.2%. Other internal nodes were scaled using a minimum time interval (0.5 Ma herein) from the oldest node crownward, following previous similar approaches (Marjanović & Laurin 2008; Gómez & Lires 2019). The age of the holotype of the new *Telmatobius* species was estimated as 12 Ma (see Geological Context). Ancestral state reconstructions were performed using stochastic character mapping (Huelsenbeck *et al.* 2003) in R v.3.6.3 (R Core Team 2013), with the 'make.simmap' function of the 'phytools' package v.6.0.99 (Revell 2012) running 1000 simulations under a three-parameter symmetrical model

(SYM). We then compared the results of ancestral reconstructions based exclusively on data from extant species to those obtained after including data from the new taxon, and also compared the states of the latter with reconstructed states of the last common ancestor of *Telmatobius*.

Institutional abbreviations. GEBCO, General Bathymetric Chart of the Oceans, Monte Carlo, Monaco; KU, Biodiversity Institute, University of Kansas, Lawrence, USA; MNHN-Bol, Museo Nacional de Historia Natural, La Paz, Bolivia; NGA, National Geospatial-Intelligence Agency, Virginia, USA; NOAA, National Oceanic and Atmospheric Administration, Washington DC, USA; SIO, Scripps Institution of Oceanography, San Diego, USA; UF, University of Florida, Florida Museum of Natural History, Gainesville, USA; USNM, National Museum of Natural History, Washington, USA.

SYSTEMATIC PALAEONTOLOGY

ANURA Fischer, 1813

NEOBATRACHIA Reig, 1958

TELMATOBIIDAE Fitzinger, 1843

Genus TELMATOBIUS Wiegmann, 1834

Type species. *Telmatobius peruvianus* Wiegmann, 1834, by monotypy.

Telmatobius achachila sp. nov.

Figures 2–7, 8A, S1

LSID. https://zoobank.org/NomenclaturalActs/67EA6A9C-F043-4AE8-9904-4B7AEE49C786

Derivation of name. Specific name derives from the substantive '*achachila'*, meaning ancestral spirit or ancient in Aymara, the native ancestral language spoken in the Altiplano region where the holotype comes from.

Holotype. Several associated but mostly disarticulated cranial and postcranial bones in block MNHN-Bol-V 012795, representing a fairly-complete, partial skeleton of a single adult male frog (Figs. 2, S1), including: partially articulated neurocraium, left premaxilla, right maxilla, both pterygoids, left quadrate-quadratojugal complex with attached fragmentary squamosal, right lower jaw, articulated bony hyoid, two presacrals, sacrum, urostyle, partially articulated pectoral girdle (only lacking right cleithrum and cartilaginus elements), both humeri radio-ulnae, and distal carpals 5-4-3, metacarpals, a phallanx, pelvic girdle, both femora, and left tibiofibula.

Locality and horizon. Achiri, north-western base of Cerro Pisakeri, *c.* 3 km south of Achiri village, Pacajes Province of La Paz Department, in the northwestern Altiplano, Bolivia. Lacustrine tuffaceous argillite level and locus ACH-14, lower part of the uppermost member (M6) of the Mauri Formation, late Middle–early Late Miocene (Prámparo *et al.* 2022).

Diagnosis. Medium-sized *Telmatobius* with an estimated total length (from the tip of the premaxilla to the end of the urostyle) around 8–9 cm; clearly distinguishable from non-*Telmatobius* anurans by the unique combination of neurocranium well ossified with relatively extensive sphenethmoid and otic capsules, with relatively long and narrow cristae parotica; paired frontoparietals distinctly separated anteriorly from one another and not reaching the antorbital plane; premaxilla and maxilla dentate, the latter lacking a distinct pterygoid process; quadrate ossified and fused to quadratojugal; lower jaw with a relatively deep dentary bearing a sharp oral margin; hyoid with posteromedial process ossifications extensively invading the hyoid plate; humerus with well-developed lateral and medial crests that merge into a single dorsal crest; tibiofibula slightly longer (*c.* 7%) than femur. In addition, compared to species of *Telmatobius* for which skeletal features are adequately known, *Telmatobius achachila* can be diagnosed within the genus by several autapomorphies, recovered as such in the phylogenetic analyses, including: long cultriform process, reaching the level of the antorbital plane (B17, c27: 0 → 1); well ossified crista parotica (GT21, c38: 0 → 1); palatine with slightly expanded medial end (GT21, c183: 0 → 1; indicated by the palatine scar on the sphenethmoid); occipital crest well developed on otic capsule (GT21, c190: 1 → 2); otic capsule with ventrolateral otic ledge completely ossified (GT21, c194: 0 → 1); small coronoid process (B17, c33: 0 → 1; GT21, c60: 1 → 0); partially fused dentary and angulosplenial (B17, c36: 0 → 1; GT21, c219: 0 → 2); hyoid plate with central mineralisation

(B17, c37: 0 → 1); sacral oblique crest sharp over diapophyses (GT21, c233: 2 → 3); and scapula with acromial cartilage ossified as an acromial process (GT21, c235: 0 → 1).

Description

The holotype consists of a well-ossified partial skeleton representing a single adult individual of *c.* 8–9 cm total (snout–urostyle) length (all bones are about the same size of those of *Telmatobius* species of this length), including most of the skull and the postcranium (Figs. 2, S1). Several osteological features, including the morphology of the hyoid and the humeri, indicate that it was a male (see below).

Cranium. Most of the neurocranium, part of the suspensorium, the right maxilla, and the left premaxilla are preserved. Except for the left premaxilla, all other cranial bones have been mechanically removed from the main block (Figs. 2B, S1). The skull, and particularly the braincase, is well ossified. Dermal bones lack ornamentation. According to the proportions of the preserved bones, the skull would have been wider than long, with large orbits and a preorbital region representing between one-fourth and one-third of the total skull length. The braincase appears to be narrow, and is estimated to be nearly one-fourth of the skull width at the level of plana antorbitale (antorbital planes).

Both otic capsules are preserved; the right one is articulated with the anterior part of the braincase and the left one is isolated but, both otic capsules are broadly invested by the parasphenoid alae ventrally (Fig. 3). Otic capsules are formed by the fusion of paired prootics and exoccipitals into otoccipitals and, when articulated, appear to contact each other along the ventral midline where they form the bony ventral margin of a roughly pentagonal foramen magnum. Whether or not the otoccipitals also contact dorsally is uncertain due to the incompleteness of their dorsomedial margins, but it is clear that the foramen magnum remains moderately separated from the skull table dorsally. Dorsolateral to the foramen magnum and near to it, a well-developed sharp and obliquely oriented occipital crest protrudes from the posterior surface of the otic capsule, almost reaching the top of the otic crest (Fig. 3A). Parallel and medial to the posteroventral part of the otic crest there is an additional posterior crest (pcr in Fig. 3A). The occipital condyles are located along the ventrolateral margins of the foramen magnum and would be separated from each other by a relatively narrow but distinct intercotylar distance when in articulation. Lateral to each occipital condyle, there is a

shallow yet well-delimited condyloid fossa where the jugular foramen (from the brain cavity; not visible in the posterior view of the otic capsule because it is concealed by the occipital condyle) and the inferior perilymphatic foramen (from the inner ear space), open extracranially. The superior perilymphatic foramen appears to open intracranially, but lies nearly in the same plane as the posterior one, being visible from a posterior and slightly lateral view. The inner ear space opens laterally through the fenestra ovalis, which is completely bounded in bone and lies relatively deep, being surrounded ventrally by a well-developed ventrolateral otic ledge (*sensu* Gómez 2016) and anteriorly by the anterior wall of the prootic. The tympanic space is roofed dorsally by a largely-ossified, relatively long and narrow crista parotica, only the distal edge of which would have been delineated in cartilage. There is no evidence of a facet for the otic ramus of the squamosal, suggesting that the latter was inconspicuous and would not have reached the otic capsule. The crista parotica has nearly parallel anterior and posterior margins, being only slightly dilated distally, and would have been directed almost laterally and slightly dorsally in the articulated skull. Dorsally on each otic capsule, the position of the anterior and posterior semicircular canals is clearly marked by well-ossified, distinct epiotic eminences, of which the posterior ones (otic crests *sensu* Maglia *et al.* 2007) are sharper than the rounded anterior ones. At their intersection, the most medial part of the anterior and posterior eminences is partially invested by the roughly squared posterolateral (paroccipital) process of the frontoparietal, which is preserved on the left otic capsule (Fig. 3C). This process bears a low, sharp ridge extending up to its posterolateral tip, which barely extends above the anteromedial part of the posterior epiotic eminence. Anterior to the contact of this process and the anterior epiotic eminence, the prootic is pierced by a tiny foramen, the identity of which is uncertain. In the anterior view, the anterior wall of the prootic bears a broad, well-delimited pterygoid facet for the medial ramus of the pterygoid (Fig. 3B). Medially to the pterygoid facet, a large prootic (trigeminal) foramen appears to be fully enclosed in prootic ossification, although this condition is uncertain because the anterior margin is broken in the left otic capsule and it is partially obscured by matrix in the right one. The presence of an operculum and stapes cannot be verified.

The sphenethmoid is also extensively ossified, with its left and right halves fully fused across the midline (Fig. 3C, D). The sphenethmoid ossification extends posteriorly up to the anterior margin of the optic foramen and anteriorly into the posterior part of the septum nasi, also invading the tectum and solum nasi. Anterolaterally, sphenethmoid ossification extends into the most proximal part of the antorbital plane and into the ridge-shaped crista

supraorbitalis at the anteromedial corner of the orbit, thereby completely enclosing the orbitonasal foramen. Dorsally, the sphenethmoid is extensive and would have been broadly exposed between the dermal roofing bones, based on the observation that the nasals (which are not preserved) left no scars on the dorsal surface of the sphenethmoid. Also, the anterior edges of the frontoparietals lie well posterior to the level of the planum antorbitale, only slightly anterior to the anterior margin of the frontoparietal fenestra (Fig. 3C). The frontoparietal fenestra, in turn, would have been only narrowly exposed between the frontoparietals, as indicated by an articulated fragment of the frontoparietal on the right side, which slightly tapers anteriorly into an irregular end. Although the other parts of frontoparietals are poorly preserved, the way in which the braincase is preserved, with right and left otic capsules disarticulated from one another, suggests that the frontoparietals would have remained unfused posteriorly.

Ventrally, the braincase is largely invested by a T-shaped parasphenoid, consisting of an anterior cultriform process and two posterior subotic alae that appear to be fused to the otic capsules (Fig. 3D). Each ala is broad, slightly expanded distally, and slightly curved posterolaterally, and having its ventral surface relatively flat except for a faint curved ridge delimiting a shallow depressed area towards the concave posterior margin. Posteriorly, the parasphenoid ends near the margin of the foramen magnum as a well-developed posteromedial process. The moderately broad, lanceolate cultriform process is relatively long, reaching the level of the plana antorbitale, and its ventral surface lacks any ridges or keels, but has a few short grooves near its anterior end. The latter would have been in tenuous contact with the palatines, as indicated by a palatine scar on the left side of the sphenethmoid (‘palf’ in Fig. 3D). This scar also shows that palatines were curved and slightly dilated at their medial ends.

The suspensorium is represented by both pterygoids and part of the left squamosal that is attached to a quadrate-quadratojugal complex (Fig. 4A, B). The pterygoids are relatively well preserved, but the medial ramus of the right element and the most anterior point of the anterior ramus of the left one are broken. Each pterygoid is a triradiate bone with a relatively gracile and long anterior ramus that is more than twice as long as either of the other two rami (Fig. 4A). The medial margin of the anterior ramus is evenly concave lengthwise, whereas the lateral margin is almost straight along its anterior half where, in life, it would have paralleled and contacted the maxilla. The anterior ramus has a tapering anterior end that would have reached the antorbital plane in the articulated skull, which is further indicated by the

proportions of the braincase and the maxilla (see below). The medial and posterior rami are almost equal in length. The medial ramus is relatively broad with a concave posterior face where the basal process of the cartilaginous palatoquadrate fitted, which in life would have articulated with the otic capsule. The posterior ramus is relatively deep and flat, thereby indicating a broad covering of the palatoquadrate up to the limits of the articular surface with the lower jaw, as also indicated by a broad pterygoid facet on the quadrate-quadratojugal complex (see below).

Only part of the left squamosal ventral ramus is preserved and is firmly attached to the quadrate-quadratojugal complex, investing the posterolateral surface of the latter and limiting the pars articularis dorsally (the part of the quadrate that articulates with the lower jaw; 'q' in Fig. 4B). Although it was found disarticulated from the rest of the skull, it is clear that the squamosal was strongly inclined anterodorsally from this point, as it matches the morphology of other species of *Telmatobius*. The articulated portion of the ventral ramus of the squamosal is moderately expanded distally and relatively flat in the quadrate region, where its medial margin is distinctly separated from and nearly parallel to the pterygoid posterior ramus, as indicated by the pterygoid facet on the quadrate-quadratojugal complex (Fig. 4B), slightly verging with it anteriorly. The quadrate is heavily ossified and broadly invested posterolaterally and medially by the squamosal and the pterygoid, respectively (Fig. 4B). The relation with the pterygoid is evidenced by a broad square facet on the medial surface of the quadrate up to its articular surface. The latter is saddle-shaped, limited by strong lateral and medial buttresses. Laterally, and fused to the quadrate, there is a small quadratojugal, the maxillary spine of which would not have been articulated extensively with the maxilla.

The right maxilla is preserved almost completely, only lacking most of a relatively delicate jugal process, but some details remain obscured by the matrix or are poorly preserved (Fig. 4C). The maxilla has a nearly straight oral margin and its labial surface is relatively smooth and devoid of ornamentation. The maxilla is dentate and has three distinct parts along most of its length: a pars palatina, directed lingually and bisecting the maxilla into a pars dentalis, extending ventrally, and a pars facialis, extending dorsally. The pars palatina extends from near the anterior tip of the bone up to the anterior end of the subtemporal fossa, indicated by an inconspicuous pterygoid process that marks the posterior-most contact of the maxilla with the palatoquadrate. The pars palatina forms a shelf that is more or less narrow and thin along most of its length, but it is somewhat thicker and blunt around the level of the antorbital plane. The pars dentalis is as long as the pars palatina and only moderately deep,

slightly decreasing in depth near its posterior end. It bore teeth all along its length, as indicated by the interdental pillars narrowly separated from one another, but the morphology of individual teeth cannot be determined. The pars facialis is relatively shallow lengthwise, being deepest in the preorbital region, decreasing in depth posteriorly along the orbital region and more abruptly along the jugal process (Fig. 4C). It bears a distinct preorbital process and an inconspicuous postorbital bump that delimits the orbital ventrolateral margin. Anteriorly, the maxilla has a squared anterodorsal margin and a low, round anteroventral process that would have abutted the premaxilla.

The left premaxilla is preserved in the main block with several associated remains on top of the left iliac shaft (see Fig. 2A), exposing its labiodorsal face and, hence, preventing description of its posteroventral surface. The dentate premaxilla is mesiodistally short (Fig. 4D) and has the same three distinct parts of the maxilla. The pars facialis is inconspicuous except for an alary process projecting posterodorsally from the middle of the pars dentalis. The alary process is relatively short, narrow at its base and slightly dilated distally, being clearly concave posteriorly where it would have lodged the prenasal cartilages. The pars palatina projects posteriorly, particularly posteromedially through a distinct lingual process that appears to have its tip broken (Fig. 4D). The maxillary margin of the premaxilla is relatively straight, supporting the inference of an abutting contact with the maxilla. Two relatively large teeth appear to remain attached to the pars dentalis, but their preservation precludes further detail.

Lower jaw. The lower jaw remains in the main block (Fig. 2A) and preserves an almost complete right dentary (partially concealed by the hyoid) partially fused with part of the angulosplenial, the latter of which lacks the articular region (Fig. 4E). Both bones invest an ossified Meckel's cartilage and remain fused to it, so there is no distinct Meckelian groove in the angulosplenial. The dentary is relatively deep lengthwise relative to most other hyloid anurans, bearing a sharp oral edge towards the symphysis, where it would have fused to the Mentomeckelian bone; however, the latter is concealed by the overlying hyoid labially and matrix lingually. In any case, it appears that the dentary surpasses dorsally the Mentomeckelian bone, forming the oral margin up to or very close to the symphysis. Posteriorly, due to fusion to the underlying elements, the limits of the dentary are barely distinguishable but for a very shallow and short groove that would indicate a remnant of a

Meckelian groove. The angulosplenial preserves leaning out from its dorsal margin, a low but moderately long coronoid process, oriented dorsolingually.

Hyoid. Part of the hyoid plate and the left and right posteromedial processes of the hyoid apparatus are well preserved in the main block (Fig. 2A), with the left process almost intact, whereas the right one, though complete, is fractured in the middle (Fig. 4F). The posteromedial processes are long and extensively ossified, being distinctly expanded at both of their ends. Their ossification invaded the hyoid plate up to the level of the bases of the posterolateral processes, but would not have progressed into them. The posteromedial processes appear to be only slightly offset from each other relative to their natural position, as the anterior end of the left process barely overlaps the right one, suggesting that a narrow strip of calcified cartilage would have persisted between their anterior ends. In addition, irregular small pieces surrounding the anterior ends of the posteromedial processes presumably correspond to calcified portions of the central region of the otherwise cartilaginous hyoid plate.

Vertebral column. Only two partially preserved presacral vertebrae were identified, along with the sacrum and the anterior portion of the urostyle, all prepared out of the main block (Figs. 2B, 5, S1). The centrum ofpresacral vertebrae is dorsoventrally compressed, and wider than long in dorsal view. A fairly complete posterior presacral vertebra (Fig. 5A, B) shows a compressed centrum with an elliptic cross section. The neural canal is large, much wider and taller than the centrum. The neural arch lamina presents the base of a distinct low and pointed neural spine. The preserved bases of the transverse processes are oriented slightly dorsally. The sacral vertebra (Fig. 5C, D) bears a distinct acute neural spine, with oblique crests that continue posterodorsally along the proximal two-thirds of the preserved left diapophysis. The left sacral diapophysis is entirely preserved; it is club-shaped, with its distal end almost twice as wide as its base, and inclined around 15° dorsally and posteriorly. The posterior articulation with the urostyle is bicondylar, with the medially inclined condyles separated by a wide gap. The anterior-most preserved portion of the urostyle (Fig. 5E–G) presents a tall neural spine with a broad and flattened anterodorsal process that narrows posteriorly into a tall dorsal crest. A pair of small knobs is present on the neural arch lateral to the spine, and anterior to the small coccygeal foramina.

Pectoral girdle. Most of the pectoral girdle is preserved, including both right and left scapulae and clavicles, the right coracoid, and the left cleithrum. The right half of the pectoral girdle is in the type block (Fig. 2A), whereas the left bones have been removed from the matrix (Fig. S1). The scapula and clavicle are strongly fused to each other, whereas the coracoid seems to have been synostotically connected to both elements (Fig. 6A). The paraglenoid cartilage is completely mineralized forming a very conspicuous paraglenoid ventral protuberance, lateral to the glenoid portion of the clavicle, and a tubercle in the anterior-most portion of the acromial margin. The clavicle is as long as the coracoid and slightly shorter than the scapula, being strongly curved anteriorly. The coracoid is almost symmetrical, with expanded glenoid and sternal portions that are twice as wide as the middle portion of the element. Its anterior margin is concave, whereas the posterior margin is nearly straight. The scapula is a triradiate element of very robust appearance. The pars acromialis is very well developed and fused to the clavicle. The anterior margin bears a conspicuous tubercle/knob (acromial process) next to the one formed by the ossified paraglenoid cartilage, and a well-developed anterior crest with an irregular margin that extends along most of the scapular shaft, resulting in a convex anterior margin of the scapula (Fig. 6A). The scapular shaft is robust. Its lateral margin, which articulates with the suprascapula, is 30% longer than the length of the shaft (as measured between the glenoid and lateral margins). The posterior margin of the shaft is concave, and the shaft itself is markedly arched dorsally. The pars glenoidalis is well developed and bears a conspicuous dorsal longitudinal crest on the internal surface (Fig. S1). The anterior portion of the left cleithrum is preserved (Fig. 6B) and bears a ventral fold that would have folded over the anterior margin of the cartilaginous suprascapula. A spina acromialis sticks out from its anterior margin, the latter of which is roughly 40% longer than the lateral margin of the scapula.

Forelimbs. Both left and right humeri and radio-ulnae are preserved, along with several autopodial elements. The right humerus and radio-ulna are preserved in the main block (Fig. 2A), whereas their left counterparts have been removed from it (Fig. S1). The humerus is robust and well ossified, including the epiphyses (Fig. 6C–E). The humeral diaphysis seems almost straight, but it presents a slight anterior and dorsal bowing that is obscured by the presence of well-developed ventral, medial, and lateral crests (Figs. 2A, 6C–E). The caput humeri (humeral head) is large and slightly compressed lateromedially, bearing two very distinct lateral and medial ventral ridges that delimit a deep longitudinal groove where the paraglenoid ridge of the pectoral girdle fits. On the lateroventral surface of the caput humeri

there is a distinct, kidney-shaped glenoid fovea (fovea capitis *sensu* Gaupp 1896; Fig. 6D), in which the medial scapulo-humeral ligament attaches in extant anurans. The medial ridge of the epiphysis is contiguous with a large ventral (deltoid) crest that projects over the proximal half of the humeral shaft (diaphysis). The margin of this crest is rugose and presents tuberosities on both sides. On its medial surface there is a well-defined medial groove (fossula dividens *sensu* Bolkay 1919) for the tendon of the coracoradialis muscle, flanked by a low tuberous paraventral crest (parietal crest). The presence of a ligamentous bridge over the medial groove is evidenced by opposing conspicuous bony knobs on ventral (deltoid) and paraventral crests ('lbrb' in Fig. 6C), representing the attachment sites of this ligament. The lateral and medial crests are very well developed, the medial one being much larger and with an irregular margin, and they project dorsally merging at midlength of the diaphysis forming a single dorsal crest that almost reaches the proximal epiphyseal margin (Fig. 6E). The humeral ball is relatively large and well-mineralised, slightly compressed mediolaterally, and flanked by a small lateral epicondyle (ectepicondyle) and a very large medial epicondyle (entepicondyle). The medial epicondyle protrudes distally beyond the distal end of the humeral ball and limits medially with a broad entepicondylar groove. The radio-ulna is about 70% the length of the humerus and its minimum width is 60% of its maximum width (at the distal end) (Fig. 6F). The olecranean process bears a well-developed medial articular facet that fits the entepicondylar groove of the humerus. The distal epiphysis bears a well-developed ulnar protuberance that clearly surpasses the polygonal radial portion of the epiphysis and is separated from it by a wide shallow groove.

Both distal carpals 5-4-3 are preserved (Figs. 2B, 6G, H, S1). These relatively large and well-ossified carpals show several anatomical features that, coupled to some metacarpals (see below), allow the reconstruction of most of the manus. In a proximal view (Fig. 6G), a large fossa occupies most of the surface of the bone forming part of the carpal volar fovea (*sensu* Gaupp 1986). Near its preaxial margin, this fossa is pierced by a large anterior carpal foramen, through which the main terminal branch of the ulnaris nerve passes in anurans. The carpal volar fovea is delimited distally by a faint transverse ridge (carpal transverse crest) that is more protruding towards the preaxial side. The facets for Distal Carpal 2, Element Y, radiale, and ulnare are distinct on the carpal side (i.e. towards the rest of carpals) along a preaxial-postaxial axis (Fig. 6G). The facet for Distal Carpal 2 has a shallowly concave palmar part and a protruding convex dorsal part that would have fitted a concavity on that unpreserved carpal. The facet for Element Y is deeply concave and relatively narrow, facing

proximally and somewhat pre-axially, whereas the radial and ulnar facets are comparatively less deep and separated from one another by a groove that formed the distal part of an intercarpal foramen. From the ulnare margin, a small but distinct process ('pem' in Fig. 6G, H) protrudes post-axially and slightly dorsally, where the extensor muscles of the ulna and digit V likely attached (Gaupp 1896). The ulnare facet is well exposed in this proximal view; it is somewhat triangular and elongate, delimits the carpal volar fovea postaxially, and has its apex towards the palmar side and bordered by a protruding buttress. This configuration, jointly with that of the ulnar portion of the radio-ulna, suggests that the unpreserved ulnare was trapezoidal and deep in the dorso-palmar axis. From the palmar face of Distal Carpal 5-4-3, distal and aligned to the palmar buttress of the ulnare facet there protrudes a round short ridge ('clcr' in Fig. 6G), most likely as a continuation of the longitudinal crest. This ridge, in turn, forms the postaxial margin of the broad saddle-shaped palmar protruding surface of Distal Carpal 5-4-3, where parts of the palmar aponeurosis typically attach (Gaupp 1896). In distal view (Fig. 6H), the process bearing the part of the facet for Distal Carpal 2 distinctly protrudes from the carpal surface. The radiale and ulnare facets are also visible in dorsal view, with the former more exposed than the latter and showing its whole rounded outline. A tiny foramen pierces the concave surface between these facets and the slightly distally protruding articular surfaces for metacarpals IV and V. The latter are mostly visible in distal view (Fig. 6H), showing their bulging, round shapes, which contrast with the more elongate articular surface for metacarpal III that protrudes dorsal to the anterior carpal foramen.

The metacarpals II–V from the right hand, plus a left metacarpal IV and a first phalanx (Figs. 2B, S1) are preserved removed from the block. Metacarpals III–V have a similar minimum width, whereas metacarpal II, although partially preserved, is clearly more robust than the other three. Metacarpal II bears a distinct proximal medial bony excrescence. Metacarpal IV is longer than III and V, which are nearly equal in length, although the latter is slightly more robust. The phalanx, considering its size and proportion with the metacarpals, seems to be the first phalanx of finger IV.

Pelvic girdle. The pelvic girdle is well preserved in the main block lying on its ventral side and partially overlaid by other bones (Fig. 2A), meaning some of its features are not visible. The pelvic girdle is completely articulated and lacks distinct sutures between bones, which, taking into account the disarticulated nature of most of the skeleton, clearly indicates that ilia and ischia are entirely fused to each other. It is likely that those bones are also fused to a

completely ossified pubis, yet it is obscured by matrix. Both ilia have their shafts fractured, and their anterior ends are broken, but it appears that they slightly curved ventrally and medially, evenly along their length, forming an open V-shaped interiliac profile in dorsal view (Fig. 7A). Iliac shafts are robust, being mediolaterally compressed at their proximal part (towards the ilial body) and slightly dorsoventrally flattened towards their distal ends (towards the ilio-sacral joint). The iliac shaft lacks a distinct dorsal crest, but a blunt and low ridge rises distally, delimiting a shallow but distinct gutter on the medial face of the shaft. The ilium has a well-developed, bell-shaped and nearly symmetrical dorsal prominence, projecting dorsolaterally at the boundary between the iliac shaft and body. On its lateral face, the dorsal prominence bears a distinctly protruding oval dorsal protuberance. Posteromedially, the ilia lack symphyseal tubercles, meaning the interiliac symphysis would have been completely ligamentous. The fused ischia moderately protrude into a median posterodorsal process capped by an ossified marginal cartilage, and have an almost straight posteroventral margin. The ischia also protrude laterally, forming well-developed posterior acetabular rims.

Hind limbs. Both femora and the left tibiofibula are preserved, removed from the block (Figs. 2B, S1). Interestingly, the right femur and the tibiofibula present different pathologies; the femur bears an osteomyelitis-like inflammation (Rothschild *et al.* 2012) of the proximal diaphysis (resulting in a diameter *c.* 44% larger than its non-pathologic counterpart) (Fig. 7B, C), whereas the tibiofibula has a healed fracture (Fig. 7D). The femur is long and gracile (length roughly 17 times its minimum width), sigmoid, and with a barely noticeable femoral crest. The femoral head is well ossified and bears a conspicuous dorsolateral trochanter (insertion of the external iliac muscle), separated from the rest of the head by a well-defined groove (insertion of the internal obturator muscle) (Fig. 7B). On the medial surface of the femoral head, there is a large groove (fovea capitis *sensu* Gaupp 1896) for the insertion of the ventral (teres) ligament (Fig. S1). The tibiofibula is slightly longer than the femur (*c.* 7%), gracile (length roughly 14 times its minimum width), and straight (Fig. 7D). Both epiphyses are well ossified, and the proximal one has a well-defined cnemial crest (*sensu* Turazzini & Gómez 2023b) that is continuous with an osseous eminentia arquata on the medial margin of the proximal end of the diaphysis.

Remarks

The holotype (MNHN-Bol-V 012795) of *Telmatobius achachila* closely resembles species of *Telmatobius* in all aspects of its skeleton, including some features formerly proposed as either typical, diagnostic, or synapomorphic for the genus (Lynch 1971, 1978; De la Riva *et al.* 2012; Barrionuevo 2017): i) frontoparietals do not reaching the antorbital plane; ii) small otic ramus of squamosal not investing crista parotica (inferred in the fossil based on the lack of a squamosal scar on the crista parotica); iii) robust parasphenoid fused to otic capsules; iv) dentate maxilla having a narrow palatal shelf and lacking a distinct pterygoid process; v) pars articularis of the palatoquadrate ossified (quadrate) and fused to quadratojugal; and vi) hyoid plate ossified up to the base of the posterolateral processes. The detailed morphology of some parts of the skeleton of *T. achachila* that has seldom been described in other anurans, such as the Distal Carpal 5-4-3 or the metacarpal II, also matches that of extant species of *Telmatobius* examined by us, but contrasts with that of most other anuran groups.

MNHN-Bol-V 012795 shows several features that are uncommon among anurans, but that clearly point to affinities with *Telmatobius*. Among these, the greatly expanded lateral and medial humeral crests in MNHN-Bol-V 012795 (Figs. 2A, 6C, 8A) can be found in males of only a few neotropical genera: *Telmatobius* (Lynch 1971, 1978; De la Riva *et al.* 2012; Fig. 8B–D), *Alsodes* (Lynch 1971, 1978:fig. 9A), *Telmatobufo* (Formas *et al.* 2001; Suazo Lara & Gómez 2022; Fig. 8E), *Leptodactylus* (*L. pentadactylus* and *L. latrans* species groups; Lynch 1971; Fig. 8F), *Rhinella* (particularly developed in species of the *R. spinulosa* species group; Guevara *et al.* 2022:fig. 3B, D), and a few hylid species in the genera *Boana* (Duellman *et al.* 1997; Fig. 8G), *Bokermannohyla* (Faivovich *et al.* 2009), *Hyloscirtus* (Duellman *et al.* 1997:fig. 4), and *Plectrohyla* (Duellman & Campbell 1992). However, *T. achachila* markedly differs in humeral morphology, including that of the lateral and medial crests, from species in all these genera except *Telmatobius* (Fig. 8). The medial and lateral crests are nearly always enlarged in males of *Telmatobius*, with only very few exceptions (see scoring of character 52 of Barrionuevo 2017), and merge into a single dorsal crest (Fig. 8A–D). MNHN-Bol-V 012795 shares with other species of *Telmatobius* the overall proportions of the humerus and its crests, including , a large ventral crest extending over half of the shaft, and in having medial and lateral crests that develop into flanges that gently merge into a single dorsal crest, but also in more detailed features, such as the large and slightly compressed humeral head bearing strong lateral and medial ventral ridges delimiting a deep groove for the paraglenoid

ridge, the kidney-shape of the glenoid fovea, and the epicondyle morphology, with a small lateral epicondyle and a very large medial epicondyle that protrudes distally beyond the distal end of the humeral ball. The coalescence of medial and lateral crests into a single dorsal crest does not occur in bufonids, hylids, and most abovementioned anurans (Fig. 8E, G), including *Alsodes* (Lynch 1978:fig. 9A), and when present it clearly differs in its configuration (Fig. 8F). In addition, *T. achachila* markedly contrasts from bufonid toads (including *Rhinella*) in having dentate premaxilla and maxilla, from hylids in its robust pectoral girdle and humerus (e.g. Maglia *et al.*, 2007; Fig. 8), from *Leptodactylus* in lacking a squamosal-prootic articulation and in having a proportionally longer pterygoid anterior ramus (Lynch 1971; Ponssa 2008), and from *Alsodes* and *Telmatobufo* in having frontoparietals not reaching the antorbital plane, ossification of hyoid posteromedial processes invading the hyoid plate, scapula with an anterior crest and fused to clavicle (variable within *Telmatobius*), and femoral crest indistinct (see character scorings of species of *Telmatobius* and *Alsodes* in datasets GT21 and B17 and of *T. achachila* in Appendix S2).

As mentioned above, we interpret that the holotype (MNHN-Bol-V 012795) represents an adult male, based on enlarged lateral and medial crests of the humerus, which are typical of males of several species of *Telmatobius* (Lavilla & Ergueta Sandoval 1999; Barrionuevo & Baldo 2009; Aguilar *et al.* 2012; De la Riva *et al.* 2012; Barrionuevo 2013; Fig. 8B–D), but also on other features related to extensive ossification and/or hypertrophied structures. Among the latter, a well-ossified pectoral girdle with a large scapular anterior crest, a robust metacarpal II, and a mineralised hyoid plate greatly invaded by posteromedial ossifications, all of which occur in the holotype, have also been regarded as typical of males in some species of *Telmatobius* (Barrionuevo 2013).

Finally, some osteological features of the holotype might indicate that *Telmatobius achachila* from Achiri was aquatic, in agreement with the lacustrine setting in which the fossils were found. Noteworthy, the combination of a mineralised hyoid plate with a relatively deep lower jaw decreasing abruptly at the symphysis has been related to inertial suction feeding in a few species of *Telmatobius*, whereas other congeners lacking these features feed underwater by means of other strategies, including compensatory suction (Barrionuevo 2016). The morphology of the symphyseal part of the lower jaw of MNHN-Bol-V 012795 cannot be established, but the combination of a relatively deep dentary bearing a sharp oral margin and a at least partially mineralised hyoid plate suggest some suction capabilities for underwater feeding.

PHYLOGENETIC ANALYSES

The parsimony analyses of the datasets GT21 and B17 recovered *Telmatobius achachila* nested within a well-supported monophyletic *Telmatobius* under all analytical conditions (Fig. 9), in agreement with the results of our taxonomic comparisons. Analyses under equal (EW) and implied (IW) weights with different values of the concavity constant *k* yielded very similar results, showing *T. achachila* nested in all cases within a large clade that is sister to the *T. verrucosus* group (represented only by *T. verrucosus* in the dataset GT21). The alsodid genera *Eupsophus* and *Alsodes* nearly always emerged as sister groups of *Telmatobius* using datasets B17 and GT21, respectively. Analysing dataset GT21, the main discrepancy was that *T. achachila* appeared as sister to *T. marmoratus* with IW (*k* = 5–9) in single MPTs (671–681 steps; CI = 0.476–0.483; RI = 0.569–0.581; Fig. S2), whereas it formed part of a polytomy with the latter and species of the *T. bolivianus* group (i.e. *T. hauthali*; *T. scrocchii*) in the strict consensus of six MPTs (671 steps; CI = 0.483; RI = 0.581) from the EW analysis (Fig. S3). Note that the *Telmatobius* sample in this dataset (seven of 62 species) is too poor to allow a more accurate analysis of relationships within the genus. Analysing dataset B17 under EW with ordered characters yielded 144 MPTs (327.079 steps; CI = 0.363; RI = 0.721), in the strict consensus of which *T. achachila* emerged in a nested position among members of the *T. bolivianus* group (Fig. S4). When characters remained unordered this clade collapsed in the strict consensus of 576 MPTs (320.108 steps; CI = 0.371; RI = 0.728), with *T. achachila* in a broad basal polytomy along some other species crownward to the node *Telmatobius* (Fig. S5), which was mainly due to *T. achachila* taking two alternate positions: either within a *T. bolivianus* group or outside the latter in a more early-branching position. The latter position agreed with the better resolved strict consensus obtained under IW (*k* = 5–7), with characters either ordered (232 MPTs of 329.332–330.332 steps; Fig. S6) or unordered (four MPTs of 322.430 steps; also with *k* = 8–9; Figs. S7, S9), in which *T. achachila* emerged crownward to the *T. verrucosus* group and to the southern taxa *T. ceiorum* and *T. stephani*, in a relatively basal polytomy with a small northern clade (*T. truebae* + *T. niger*) and a very large clade including the remaining species of *Telmatobius*. Analysis of B17 under IW (*k* = 8–9) with characters ordered (100 MPTs of 328.332 steps; CI = 0.361; RI = 0.720) yielded similar results as those under EW, with *T. achachila* nested within members of the *T. bolivianus* group (Fig. S8). A summary of the results using datasets B17 and GT21 is reported over the

strict consensus of four MPTs (Fig. 9A) and the single MPT (Fig. 9B), respectively, obtained under implied weighting (with $k = 7$) and multistate characters unordered.

In all of our analyses monophyly of *Telmatobius* was supported by ten and four unambiguous osteological synapomorphies using the datasets GT21 and B17, respectively, most of which can be seen in the holotype of *T. achachila*, as follows: anterior margin of frontoparietals not reaching the level of the antorbital plane (B17, c4: 0 → 1); quadrangular posterolateral process of frontoparietal partially overlapping the epiotic eminence (GT21, c162: 0 → 1); reduced otic ramus of squamosal (GT21, c9: 1 → 0; B17, c31: 1 → 0; inferred from the morphology of the crista parotica); moderately developed pars jugalis of quadratojugal (GT21, c53: 2 → 1); reduced pterygoid process of maxilla (GT21, c213: 1 → 0); well-developed anterior crest on scapula (GT21, c114: 1 → 2); greatly enlarged lateral and medial crests of the humerus (GT21, c242: 0 → 1). In addition, several transformations optimised as autapomorphies of *T. achachila* (all visible in the holotype) include: slightly expanded medial end of palatine (GT21, c183: 0 → 1; evidenced by the palatine scar on the sphenethmoid); long cultriform process of parasphenoid (B17, c27: 0 → 1); well-developed, sharp occipital crest on exoccipital (GT21, c190: 1 → 2); completely ossified ventrolateral otic ledge (GT21, c194: 0 → 1); dentary sutured (or partially fused) to angulosplenial (GT21, c219: 0 → 2; B17, c36: 0 → 1); small coronoid process (B17, c33: 0 → 1; GT21, c60: 1 → 0); mineralised hyoid plate (B17, c37: 0 → 1); ossified acromial cartilage on scapula (GT21, c235: 0 → 1).

ANCESTRAL SUBSTRATE PREFERENCE, HABITAT, AND ELEVATION

Stochastic character mapping of substrate preference, main habitat, and mean elevation, alternatively excluding or including data from *Telmatobius achachila*, yielded roughly similar results for most nodes within *Telmatobius* (Fig. 10A). However, some important differences existed in the reconstructions for the last common ancestor of *Telmatobius.* When including data from extant taxa only, the last common ancestor of *Telmatobius* was reconstructed as a semi-aquatic (53.2%) frog that inhabited forests (99.3%) at mid-high elevations of 2500–3500 m (37.1%), although optimisations of substrate preference and elevation range were quite equivocal, since the likelihood of a semi-aquatic habit was only a little higher than an aquatic habit (45.1%) and mid-low and high altitude ranges had only slightly lower likelihoods

(36.5% and 36.4%, respectively). When data from *T. achachila* were considered, a forest habitat was also recovered with a high probability (99.4%) as the ancestral habitat for *Telmatobius*, but an aquatic habit (65.9%) and a mid-low altitude range (71.8%) were optimised as largely more probable than their respective alternative states (Fig. 10A). In addition, data from *T. achachila* also impacted the reconstruction of the elevation range at which the last common ancestor of the *T. bolivianus* and *T. marmoratus* species groups might have lived, recovering high- (49.5%) and mid-high (65.2%) altitude ranges as the most probable states excluding or including data of *T. achachila*, respectively.

DISCUSSION

The genus *Telmatobius* is speciose and its referred extant species are distributed throughout the Andean and Puna highlands from Ecuador to San Juan Province of Argentina (De la Riva *et al.* 2010), but despite this, its fossil record is almost null. An indeterminate species of *Telmatobius* has only recently been reported from the Quaternary of the Antofagasta Region of Chile, based on several isolated fossils still undescribed (Figueroa-Bravo *et al.* 2022). The discovery of *T. achachila*, a new extinct species of *Telmatobius* from late Middle to early Late Miocene of the Bolivian Altiplano known from cranial and postcranial bones, is a significant and noteworthy achievement that enhances our understanding of the morphology and evolutionary history of this Andean group.

Allocation of *Telmatobius achachila* to crown-group *Telmatobius* is grounded on several cranial and postcranial features, including several synapomorphies of the genus recovered as such in the present and former cladistic analyses (Barrionuevo 2017; Gómez & Turazzini 2021a; see phylogenetic analyses results). The many features shared by *T. achachila* and extant species of the genus indicate that their overall skeletal anatomy is evolutionary conservative, remaining almost unchanged for at least 12 Ma, in agreement with previous statements regarding external morphology (Benavides *et al.* 2002). It is worth noting that very few of these osteological features have been considered in most systematic studies of *Telmatobius* (e.g., Lynch 1971; Trueb 1979; Wiens 1993; Lavilla & Barrionuevo 2005; Aguilar *et al.* 2012; De la Riva *et al.* 2012; Barrionuevo 2017). Additionally, important intraspecific variation has been reported for some skeletal traits (Lobo Gaviola 1989; De la Riva 2005; Lavilla & Barrionuevo 2005; Sinsch *et al.* 2005; Barrionuevo 2013). For these

reasons, osteology in general has often been regarded as of limited systematic value for inferring phylogenetic relationships or establishing taxonomic boundaries in the group (Sinch *et al.* 2005; De la Riva *et al.* 2010; Sáez *et al.* 2022). However, our findings agree with those of Barrionuevo (2017) and De la Riva *et al.* (2012), demonstrating that osteological characters can be useful in the systematics of *Telmatobius*. Given that resolving evolutionary relationships of *Telmatobius*, both among component species and among other hyloid neobatrachians, have proven to be elusive based either on external morphology or on molecular data (e.g., De la Riva *et al.* 2012; Barrionuevo 2017; Streicher *et al.* 2018; Sáez *et al.* 2022), osteological data emerges as a particularly informative source of characters for the group (De la Riva *et al.* 2012; Barrionuevo 2017). However, there is still a paucity of osteological data for several parts of the skeleton and for most species of *Telmatobius* (De la Riva *et al.* 2012; Barrionuevo 2017), despite the growing body of osteological descriptions available in the literature (Lynch 1971, 1978; Trueb 1979; Laurent & Lavilla 1986; Lavilla & Laurent 1988; Lobo Gaviola 1989; Wiens 1993; De la Riva 1994; Lavilla & Ergueta Sandoval 1995, 1999; Benavides *et al.* 2002; Cuevas & Formas 2002; De la Riva & Harvey 2003; Formas *et al.* 2003, 2006; Lavilla & Barrionuevo 2005; Sinsch *et al.* 2005; Barrionuevo & Baldo 2009; Aguilar *et al.* 2012; De la Riva *et al.* 2012; Barrionuevo 2013, 2018; Báez & Gómez 2018).

Telmatobius achachila has a unique combination of features, including several autapomorphies that set it apart from other species of *Telmatobius*, and as such justifying the erection of a new species. Some of these diagnostic features appear to be otherwise unique to *T. achachila* within the genus, or at least among the congeners whose osteology is adequately known, such as the slightly expanded medial ends of palatines (GT21, c183: 0 → 1), the well-developed occipital crest on exoccipital (GT21, c190: 1 → 2), the dentary and angulosplenial partially fused (B17, c36: 0 → 1; GT21, c219: 0 → 2), and the scapula with an ossified acromial cartilage (GT21, c235: 0 → 1). These features could be interpreted as the result of hyperossification and/or peramorphic development of the skeleton relative to other species of *Telmatobius* (Báez & Gómez 2018; Barrionuevo 2018), converging in some aspects with ceratophryids, and more particularly with species of *Lepidobatrachus* (Fabrezi 2006; Gómez & Turazzini 2021a; Turazzini & Gómez 2023a). Alternatively, they could have been inherited from a common ancestor, since a sister-group relationship between *Telmatobius* and Ceratophryidae has previously been proposed by some molecular-based studies (e.g., Grant *et al.* 2006; Fouquet *et al.* 2013; de Sá *et al.* 2014), although most recent studies have pointed to

a more distant relationship between them (e.g., Roelants *et al.* 2007; Pyron 2014; Feng *et al.* 2017; Hutter *et al.* 2017; Streicher *et al.* 2018; Hime *et al.* 2021). Other features recovered as autapomorphic of *T. achachila*, although not unique, are shared with very few species within *Telmatobius*, including a small coronoid process (B17, c33: 0 → 1; GT21, c60: 1 → 0) and a partially mineralised hyoid plate (B17, c37: 0 → 1). Aside from occurring in *T. achachila*, these features occur jointly only in a few species of the *T. marmoratus* species group, including *T. marmoratus* and *T. culeus* from the Altiplano, which might account for the phylogenetic position recovered with the dataset GT21, yet results with the densely taxonomically sampled dataset B17 show that these similarities are better explained as convergences.

Interestingly, both *Telmatobius marmoratus* and *T. culeus* are aquatic inhabitants of Lake Titicaca of the Altiplano of Bolivia and Peru, although the former also thrives in streams, small lakes, and other wetlands across the Altiplano (De la Riva 2005). Similarly, *T. achachila* appears to be an aquatic frog that lived in a lake at a mid-low elevation (no more than 2000 m ASL) according to geological and palynological data (Garzione *et al.* 2017; Boschman 2021; Prámparo *et al.* 2022). Curiously, the region of Achiri where the fossils were found is currently both at a similar height (3960 m ASL) and *c.* 75 km south to the southern shore of the Lake Titicaca (3820 m ASL; Fig. 1), although when *T. achachila* lived it was located at a much lower elevation than today (*c.* 1600 m ASL; Gregory-Wodzicki *et al.* 1998; Garzione *et al.* 2017; Martínez *et al.* 2020; Prámparo *et al.* 2022). Since *T. achachila* appears as distantly related to these species, lacking some features recovered as synapomorphic of the *T. marmoratus* species group (and adjacent nodes) such as the greater anterior extent of frontoparietals (B17, c4: 1 → 0) and otic ramus of squamosal (B17, c31: 0 → 1) (Barrionuevo 2017; this study), it is likely that convergences between them are related to environmental adaptation to an aquatic life. Convergences in aquatic frogs have previously been stressed (Emerson 1988; Moen *et al.* 2016; Gómez & Lires 2019), including cases between distantly related taxa such as paradoxical frogs and pipids (Turazzini & Gómez 2023b), but also between sister lineages within Pipidae (Gómez & Pérez-Ben 2019) and even between species of *Telmatobius* (Barrionuevo 2016). Among the latter, a mineralised hyoid plate, coupled with certain features of the lower jaw, has been linked to inertial suction during underwater feeding (Barrionuevo 2016). A mineralised hyoid plate has been reported in several aquatic *Telmatobius* (Barrionuevo 2016, 2017), including *T. macrostomus* that also inhabits large lakes, yet in this case it is not coupled with particular lower jaw modifications. In addition,

the small coronoid process in *T. achachila* and the *T. marmoratus* species group might also be related to a similar development and insertion of adductor mandibulae muscles (= levator mandibulae; Johnston 2011), involved in adducting the lower jaw, but their relation to inertial suction feeding remains unexplored. Interestingly, the only other anurans that have been reported as capable of inertial suction are the hymenochirine pipids (Sokol 1969; Carreno & Nishikawa 2010), which appear to have a single adductor mandibulae (Sokol 1969) and a coronoid process, although not particularly small, distinctly smaller than that of other pipids (Cannatella & Trueb 1988:fig. 5; ROG pers. observ.).

Phylogenetic analyses of dataset B17 under most analytical conditions recovered *T. achachila* as an early branch within the *Telmatobius* tree, crownward to the divergence of the *T. verrucosus* species group (Fig. 9A), which, taking into account the relatively old age of the fossils, makes *T. achachila* a key taxon for understanding the early evolution of the group with an important potential impact in the reconstruction of ancestral conditions (Fig. 9B). It should be noted, though, that the inclusion of *T. achachila* into the data matrices of Barrionuevo (2017) and Gómez and Turazzini (2021a) does not significantly alter the topologies obtained in those studies. However, a few differences exist regarding the dataset B17, since the strict consensus from the analysis under equal weights with multistate characters unordered is much less resolved than the one reported by Barrionuevo (2017:fig. 2), because in our analysis the *T. bolivianus* species group collapses (Fig. 9A) due to alternative positions of *T. achachila* (see results). Some other differences with the topology reported by Barrionuevo (2017) are related with different analytical conditions (e.g. treatment of multistate characters), of which the most notable is the relatively basal position of a clade formed by *T. ceiorum* and *T. stephani* (Fig. 9A), lying well outside the *T. bolivianus* species group to which they were formerly located (Barrionuevo 2017). It would be worth testing more thoroughly the phylogenetic position of *T. ceiorum* and *T. stephani*, but this is beyond the scope of the present work. Interestingly, these two semi-aquatic/aquatic species inhabit montane forests (Yungas) of northwestern Argentina at elevations below 2300 m ASL (Lavilla & Barrionuevo 2005), contrasting with most other members of the *T. bolivianus* species group that either inhabit highland streams of the Puna/Altiplano or at higher elevations in the montane forests of Bolivia (De la Riva 2005; Lavilla & Barrionuevo 2005; De la Riva *et al.* 2010).

Telmatobius achachila might have also inhabited forests at relatively mid-low elevations (below 2000 m ASL), based on varied sources of geological and palynological data

from which it is inferred that forests with conifers (Araucariaceae and Podocarpaceae), legumes, and *Polylepis* spread in the central Altiplano of Bolivia during Middle–early Late Miocene times (Gregory-Wodzicki 2002; Garzione *et al.* 2017; Boschman 2021; Prámparo *et al.* 2022; Fig. 10B). These ancient floras, and others from the Miocene of southern Peru (Martínez *et al.* 2020), share several components with extant montane forests now restricted along the Andean eastern slopes (Gregory-Wodzicki 2002; Prámparo *et al.* 2022; Fig. 10B). The phylogenetic reconstructions including data from *T. achachila* point to ancestral *Telmatobius* also inhabiting in wetlands surrounded by forests at relatively mid-low elevations (below 2500 m ASL), despite extant species in the early-diverging *T. verrucosus* species group being found at elevations up to 3500–4000 m ASL (Wiens 1993; De la Riva 2005; Aguilar *et al.* 2012). This agrees with the forest origin proposed for the anuran species of the Andean highlands (Duellman 1979; Cei 1986; Lynch 1986; De la Riva *et al.* 2010) and the 'Dynamic-Continent Hypothesis' of Lynch (1986), which predicts that populations began to differentiate as the pre-Andean landscape formed and continued to differentiate as they were further uplifted during Andean rises, and fits well the speciation model proposed for *Telmatobius* based on molecular data (De la Riva *et al.* 2010; Fig. 10). It is likely that ancestral *Telmatobius* began to differentiate in a low-elevated forest habitat in what today is the Central Altiplano during the Early–Middle Miocene, very similar to the inferred palaeoenvironment where *T. achachila* lived (Prámparo *et al.* 2022). At this time, there would have been a forested corridor along the emerging highlands of the Altiplano (Gregory-Wodzicki 2002; Martínez *et al.* 2020; Prámparo *et al.* 2022) that allowed dispersal of early populations northward and southward in similar environments. The marked uplift of the Altiplano and eastern Cordillera during the Late Miocene produced strong climatic and environmental changes in the region (Garzione *et al.* 2017; Boschman 2021), which in turn would have caused severe fragmentation of existing frog populations (De la Riva *et al.* 2010). These early populations either survived in the montane forests in the northern Andes of Peru/Ecuador and along the eastern Cordillera south to the Yungas of Argentina (their descendants would be species of the *T. verrucosus* and *T. bolivianus* species groups, plus several early-diverging lineages), or adapted to the new drier highland conditions of the Altiplano/Puna (lineages represented today by species of the *T. marmoratus* and *T. macrostomus* species groups). The presence of *T. achachila* in the late Middle–early Late Miocene of the central Altiplano and the reconstructed ancestral environmental conditions for *Telmatobius* (Fig. 10A) support this biogeographic scenario, although it will remain

speculative until more palaeontological data come to light and can be integrated in quantitative biogeographical studies.

A prerequisite for such an enterprise is an adequate timing of the phylogeny of *Telmatobius*, but to date only a few studies have tackled this issue (De la Riva *et al.* 2010; Sáez *et al.* 2014). These studies have estimated divergence times for *Telmatobius* and some of its internal nodes based on Bayesian approaches and a relaxed molecular clock, but since no fossils of *Telmatobius* were known at that time to be used as calibration points, they relied entirely on constant nucleotide substitution rates of the *cytochrome b* gene reported in the literature (Mueller 2006), obtaining disparate results under different rates for older nodes (De la Riva *et al.* 2010; Fig. 10A). The estimated mean divergence time of crown group *Telmatobius* was as old as 20 Ma (under a slow rate of 1%) to as recent as 10 Ma (under a fast rate of 2%) with large confidence intervals in all cases (De la Riva *et al.* 2010; Fig. 10A). It is noteworthy that the inclusion of *T. achachila* in the phylogeny of *Telmatobius* provides a time-adjusted tree that is highly congruent with the mean estimated divergence times based on a medium-slow nucleotide substitution rate (De la Riva *et al.* 2010; Fig. 10A). To be considered as a reliable calibration point, a fossil should have a well-estimated age and its systematic relationships need to be supported on apomorphies (Parham *et al.* 2012), conditions that *T. achachila* fulfil satisfactorily. Therefore, *T. achachila* emerges as an excellent calibration point for crown group *Telmatobius* that helps in timing the evolutionary history of the group.

CONCLUSION

Telmatobius achachila sp. nov. from the late Middle–earliest Late Miocene of Achiri, at 3960 m ASL in the Bolivian Altiplano, constitutes the first described fossil of the speciose Andean genus *Telmatobius*. Phylogenetic analyses confirm the new species as part of the crown group, which, coupled with its accurate stratigraphic provenance and well-delimited (and relatively old) age, make it a reliable and crucial calibration point to timing the evolutionary history of these highland, mostly aquatic frogs. The skeleton of *T. achachila* indicates that several of the osteological peculiarities of extant *Telmatobius* already evolved some 12 Ma ago, including some that might be linked to their aquatic lifestyle. The finding of *T. achachila* in Achiri further provides key data that allowed a more accurate reconstruction of ancestral

habitats and elevation ranges of *Telmatobius*, agreeing with the postulated ancestral conditions in which these frogs might have first evolved (Duellman 1979; Cei 1986; Lynch 1986; De la Riva *et al.* 2010). This discovery adds to the scarce evidence of a humid tropical Bolivian Altiplano just prior to the critical uplift of the area and the drastic climate deterioration which occurred in Late Miocene times onward, leading to the hostile highland-steppe environments reigning today.

Acknowledgements. We warmly acknowledge Michel Séranne, for participating in the 2022 field campaign at Achiri, Pomata-Ayte, and Choquecota, and sharing his knowledge on Andean geology and tectono-sedimentary history. Fieldwork in the Bolivian Altiplano has been carried out in the framework of an ongoing cooperation agreement (N◦864/2014) between the MNHN-Bol (La Paz, Bolivia), the *Institut des Sciences de l'Évolution de Montpellier* (France) and the CCT-CONICET (Mendoza, Argentina). This research was also supported by the National Geographic Society (NGS EC-44712R-18 [AB] and NGS 9971-16 [FP]), the ECOS-SUD/FONCyT international program (2015-2017; FP and POA), an "Investissements d'Avenir" grant managed by the French *Agence Nationale de la Recherche* (ANR) in the framework of the LabEx CEBA (ANR-10-LABX-25-01; POA and LM). This is a contribution of the Paltiplano project that has received financial support from the French *Centre National de la Recherche Scientifique* (CNRS) through the *Mission pour les initiatives transverses et interdisciplinaires* (MITI) program (SF and LM). We thank the Willi Hennig Society for the free access to the TNT software package. We acknowledge the continued support of Universidad de Buenos Aires and CONICET. We also thankfully acknowledge the contribution of the editors, J. Gardner (Royal Tyrrell Museum of Palaeontology), and an anonymous reviewer for their valuable comments and suggestions.

Author contributions. **Conceptualisation** ROG; **Data Curation** ROG, TV, GFT, RAF, BMQ, POA; **Formal Analysis** ROG; **Funding Acquisition** POA, LM, AB, FP, SF; **Investigation** ROG, TV, GFT, POA; **Field Acquisition** LM, RAF, AB, MFM, BMQ, MBP, SF, PM, FP, POA; **Methodology** ROG, TV; **Project Administration** POA, LM, AB, FP, SF; **Resources** ROG, POA; **Supervision** ROG, POA; **Validation** ROG, GFT; **Visualization** ROG, TV; **Writing – Original Draft Preparation** ROG, TV, GFT, POA; **Writing – Review & Editing** ROG, TV, GFT, LM, RAF, AB, MFM, BMQ, MBP, SF, PM, FP, POA.

DATA ARCHIVING STATEMENT

Phylogenetic data for this study are available in Morpho-Bank (O'Leary & Kaufman 2012): https://doi.org/10.7934/P2723; https://doi.org/10.7934/P4531. This published work and the nomenclatural acts it contains have been registered with ZooBank: https://zoobank.org/References/ 6888D20A-7FF8-409F-9C1F-7E760575A74F

Editor. Marcello Ruta

SUPPORTING INFORMATION

Additional Supporting Information can be found online (https://doi.org/10.1002/spp2.1543):

Appendix S1. List of comparative materials.

Appendix S2. Character scoring of *Telmatobius achachila*

Appendix S3. Substrate preference, habitat, and mean elevation of extant *Telmatobius*.

Appendix S4. Phylogenetic trees.

Table S1. List of comparative specimens with links to digital material.

REFERENCES

AGUILAR, C. and VALENCIA, N. 2009. Relaciones filogenéticas entre telmatobiinidos (Anura, Ceratophryidae, Telmatobiinae) de los Andes centrales basado en la morfología de los estados larval y adultos. *Revista Peruana de Biología*, **16**, 43–50.

AGUILAR, C., CATENAZZI, A., VENEGAS, P. J. and SIU-TING, K. 2012. Morphological variation of *Telmatobius atahualpai* (Anura: Telmatobiidae) with comments on its phylogenetic relationships and synapomorphies for the genus. *Phyllomedusa*, **11**, 37–49.

BÁEZ, A. M and GÓMEZ, R. O. 2018. Dealing with homoplasy: osteology and phylogenetic relationships of the bizarre neobatrachian frog *Baurubatrachus pricei* from the Upper Cretaceous of Brazil. *Journal of Systematic Palaeontology*, **16**, 279–308.

BARCELOS, L. A. and DOS SANTOS, R. O. 2022. The lissamphibian fossil record of South America. *Palaeobiodiversity and Palaeoenvironments*, published online 28 June. https://doi.org/10.1007/s12549-022-00536-0

BARRIONUEVO, J. S. 2013. Osteology and postmetamorphic development of *Telmatobius oxycephalus* (Anura: Telmatobiidae) with an analysis of skeletal variation in the genus. *Journal of Morphology*, **274**, 73–96.

BARRIONUEVO, J. S. 2016. Independent evolution of suction feeding in Neobatrachia: feeding mechanisms in two species of *Telmatobius* (Anura: Telmatobiidae). *Anatomical Record*, **299**, 181–196.

BARRIONUEVO, J. S. 2017a. Frogs at the summits: phylogeny of the Andean frogs of the genus *Telmatobius* (Anura, Telmatobiidae) based on phenotypic characters. *Cladistics*, **33**, 41–68.

BARRIONUEVO, J. S. 2017b. Project 2723: Frogs at the summits: phylogeny of the Andean frogs of the genus *Telmatobius* (Anura, Telmatobiidae) based on phenotypic characters. MorphoBank, P2723. https://doi.org/10.7934/P2723

BARRIONUEVO, J. S. 2018. Growth and cranial development in the Andean frogs of the genus *Telmatobius* (Anura: Telmatobiidae): exploring the relation of heterochrony and skeletal diversity. *Journal of Morphology*, **279**, 1269–1281.

BARRIONUEVO, J. S. and BALDO, D. 2009. Description of the tadpoles of *Telmatobius platycephalus* and *Telmatobius pinguiculus* from montane regions of Argentina. *Herpetological Journal*, **19**, 21–27.

BENAVIDES, E., ORTIZ, J. C. and SITES, J. W. J. 2002. Species boundaries among the *Telmatobius* (Anura: Leptodactylidae) of the Lake Titicaca Basin: allozyme and morphological evidence. *Herpetologica*, **58**, 31–55.

BOLKAY, S. J. 1919. Osnove uporedne osteologije anurskih batrahija sa dodatkom o porijeklu Anura i sa slikom narajnova sistema istih. *Glasnik Zemaljskov Muzeja Bosni Herzegovini*, **31**, 277–353.

BOSCHMAN, L. M. 2021. Andean mountain building since the Late Cretaceous: a paleoelevation reconstruction. *Earth-Science Reviews*, **220**, 103640.

BRUNETTI, A. E., MUÑOZ SARAVIA, A., BARRIONUEVO, J. S. and REICHLE, S. 2017. Silent sounds in the Andes: Underwater vocalizations of three frog species with reduced tympanic middle ears (Anura: Telmatobiidae: *Telmatobius*). *Canadian Journal of Zoology*, **95**, 335–343.

BUSER, T. J., BOYD, O. F., CORTÉS, Á., DONATELLI, C. M., KOLMANN, M. A., LUPARELL, J. L., PFEIFFENBERGER, J. A., SIDLAUSKAS, B. L. and SUMMERS, A. P. 2020. The natural historian's guide to the CT galaxy: step-by-step instructions for preparing and analyzing computed tomographic (CT) data using cross-platform, open access software. *Integrative Organismal Biology*, **2**, obaa009.

CANNATELLA, D. C. and TRUEB, L. 1988. Evolution of pipoid frogs: intergeneric relationships of the aquatic frog family Pipidae (Anura). *Zoological Journal of the Linnean Society*, **94**, 1–38.

CARRENO, C. A. and NISHIKAWA, K. C. 2010. Aquatic feeding in pipid frogs: the use of suction for prey capture. *Journal of Experimental Biology*, **213**, 2001–2008.

CEI, J. M. 1986. Speciation and adaptative radiation in Andean *Telmatobius* frogs. 374–386. *In* VUILLEUMIER, F. AND MONASTERIO, M. (eds). *High Altitude Tropical Biogeography*. Oxford University Press, New York/Oxford,

CUEVAS, C. C. and FORMAS, J. R. 2002. *Telmatobius philippii*, una nueva especie de rana acuática de Ollagüe, norte de Chile (Leptodactylidae). *Revista Chilena de Historia Natural*, **75**, 245–258.

DE LA RIVA, I. 1994. A new aquatic frog of the genus *Telmatobius* (Anura: Leptodactylidae) from Bolivian cloud forests. *Herpetologica*, **50**, 38–45.

DE LA RIVA, I. 2005. Bolivian frogs of the genus *Telmatobius*: synopsis, taxonomic comments, and description of a new species. 65–101. *In* Lavilla, E. O. and De la Riva, I. (eds). *Estudios sobre las Ranas Andinas de los Géneros* Telmatobius *y* Batrachophrynus *(Anura: Leptodactylidae)*. *Vol. 7*. Asociación Herpetológica Española, Valencia, Spain, 349 pp.

DE LA RIVA, I. and HARVEY, M. 2003. A new species of *Telmatobius* from Bolivia and a redescription of *T. simonsi* Parker, 1940 (Amphibia: Anura: Leptodactylidae). *Herpetologica*, **59**, 127–142.

DE LA RIVA, I., GARCÍA-PARÍS, M. and PARRA-OLEA, G. 2010. Systematics of Bolivian frogs of the genus *Telmatobius* (Anura, Ceratophryidae) based on mtDNA sequences. *Systematics and Biodiversity*, **8**, 49–61.

DE LA RIVA, I., TRUEB, L. and DUELLMAN, W. E. 2012. A new species of *Telmatobius* (Anura: Telmatobiidae) from Montane forest Southern Peru, with a review of osteological features of the genus. *South American Journal of Herpetology*, **7**, 91–109.

DE SÁ, R. O., GRANT, T., CAMARGO, A., HEYER, W. R., PONSSA, M. L. and STANLEY, E. 2014. Systematics of the neotropical genus *Leptodactylus* Fitzinger, 1826 (Anura: Leptodactylidae): phylogeny, the relevance of non-molecular evidence, and species accounts. *South American Journal of Herpetology*, **9** (Special Issue 1), S1–S128.

DUELLMAN, W. E. 1979. The herpetofauna of the Andes: patterns of distribution, origin, differentiation, and present communities. 371–459. *In* DUELLMAN, W. E. (ed.). *The South American Herpetofauna: its Origin, Evolution, and Dispersal*. *Museum of Natural History, University of Kansas, Monograph 7.* University of Kansas Printing Service, Lawrence, 485 pp.

DUELLMAN, W. E. and CAMPBELL, J. A. 1992. Hylid frogs of the genus *Plectrohyla*: systematics and phylogenetic relationships. *Miscellaneous publications Museum of Zoology, University of Michigan*, **181**, 1–32.

DUELLMAN, W. E., DE LA RIVA, I. and WILD, E. R. 1997. Frogs of the *Hyla armata* and *Hyla pulchella* Groups in the Andes of South America, with definitions and analyses of phylogenetic relationships of andean groups of *Hyla*. *Scientific Papers*, **3**, 1–41.

EMERSON, S. B. 1988. Convergence and morphological constraint in frogs: variation in postcranial morphology. *Fieldiana Zoology*, **43**, 1–19.

FABREZI, M. 1992. El carpo de los anuros. *Alytes*, **10**, 1–29.

FABREZI, M. 2006. Morphological evolution in Ceratophryinae (Anura, Neobatrachia). *Journal of Zoological Systematics and Evolutionary Research*, **44**, 153–166

FABREZI, M. and ALBERCH, P. 1996. The carpal elements of anuras. *Herpetologica*, **52**, 188–204.

FAIVOVICH, J., LUGLI, L., LOURENÇO, A. C. C. AND HADDAD, C. F. 2009. A new species of the *Bokermannohyla martinsi* group from central Bahia, Brazil with comments on *Bokermannohyla* (Anura: Hylidae). *Herpetologica*, **65**, 303–310.

FEDOROV, A., BEICHEL, R., KALPATHY-CRAMER, J., FINET, J., FILLION-ROBIN, J. C., PUJOL, S., BAUER, C., JENNINGS, D., FENNESSY, F., SONKA, M. and BUATTI, J. 2012. 3D Slicer as an image computing platform for the Quantitative Imaging Network. *Magnetic Resonance Imaging*, **30**, 1323–1341.

FENG, Y.-J., BLACKBURN, D. C., LIANG, D., HILLIS, D. M., WAKE, D. B., CANNATELLA, D. C. and ZHANG, P. 2017. Phylogenomics reveals rapid, simultaneous diversification of three major clades of

Gondwanan frogs at the Cretaceous–Paleogene boundary. *Proceedings of the National Academy of Sciences of the United States of America*, **114**, E5864–E5870.

FERNÁNDEZ-MONESCILLO, M., ANTOINE, P.-O., MAMANI QUISPE, B., MÜNCH, P., ANDRADE FLORES, R., MARIVAUX, L. and PUJOS, F. 2019. Multiple skeletal and dental pathologies in a late Miocene mesotheriid (Mammalia, Notoungulata) from the Altiplano of Bolivia: palaeoecological inferences. *Palaeogeography Palaeoclimatology, Palaeoecology*, **534**, 109297.

FIGUEROA-BRAVO, C. P., GUTSTEIN, C. S., LIZAMA-CATALÁN, A. and LABARCA, R. 2022. Nuevo yacimiento con vertebrados Pleistocenos del desierto de Atacama. *Segundo Congreso Chileno de Paleontología, San Vicente de Tagua Tagua, Chile, Abstracts*, **1**, 14.

FITZINGER, L. J. F. J. 1843. *Systema Reptilium. Fasciculus Primus. Amblyglossae*. Braumüller et Seidel, Wien, 106 pp.

FISCHER, G. 1813. *Zoognosia tabulis synopticis illustrata, in usum praelectionum Academiae Imperialis Medico-Chirurgicae Mosquensis edita. Volume 1. Third edition*. Nicolai Sergeidis Vsevolozsky, Moscow, i–xiv, 464 pp.

FORMAS, J. R., NÚÑEZ, J. J. and BRIEVA, L. M. 2001. Osteología, taxonomía y relaciones filogenéticas de las ranas del género *Telmatobufo* (Leptodactylidae). *Revista Chilena de Historia Natural*, **74**, 365–387.

FORMAS, J. R., BENAVIDES, E., and CUEVAS, C. 2003. A new species of *Telmatobius* (Anura: Leptodactylidae) from Río Vilama, northern Chile, and the redescription of *T. halli* Noble. *Herpetologica*, **59**, 253–270.

FORMAS, J. R., CUEVAS, C. and NUNEZ, J. J. 2006. A new species of *Telmatobius* (Anura, Leptodactylidae) from Northern Chile. *Herpetologica*, **62**, 173–183

FOUQUET, A., BLOTTO, B. L., MARONNA, M. M., VERDADE, V. K., JUNCÁ, F. A., DE SÁ, R. O. and RODRIGUES, M. T. 2013. Unexpected phylogenetic positions of the genera *Rupirana* and *Crossodactylodes* reveal insights into the biogeography and reproductive evolution of leptodactylid frogs. *Molecular Phylogenetics and Evolution*, **67**, 445–457.

FROST, D.R. 2023. Amphibian Species of the World: an Online Reference. Version 6.1 (03/05/2023). Electronic Database accessible at https://amphibiansoftheworld.amnh.org/index.php. American Museum of Natural History, New York, USA.

GARZIONE, C. N., MCQUARRIE, N., PEREZ, N. D., EHLERS, T. A., BECK, S. L., KAR, N., EICHELBERGER, N., CHAPMAN, A. D., WARD, K. M., DUCEA, M. N. and LEASE, R. O. 2017. Tectonic evolution of the Central Andean plateau and implications for the growth of plateaus. *Annual Review of Earth and Planetary Sciences*, **45**, 529–559.

GAUDIN, T. J., BOSCAINI, A., MAMANI QUISPE, B., ANDRADE FLORES, R., FERNÁNDEZ-MONESCILLO, M., MARIVAUX, L., ANTOINE, P.-O., MÜNCH, P. and PUJOS, F. 2022. Recognition of a new nothrotheriid genus (Mammalia, Folivora) from the early late Miocene of Achiri (Bolivia) and the taxonomic status of the genus *Xyophorus*. *Historical Biology*, published online 24 May. https://doi.org/10.1080/08912963.2022.2075744

GAUPP, E. 1896. *Ecker's und Wiedersheim's Anatomie des Frosches*. Friedrich Vieweg and Son, Braunschweig, 227 pp.

GOLOBOFF, P. A. 1993. Estimating character weights during tree search. *Cladistics*, **9**, 83–91.

GOLOBOFF, P. A. and CATALANO, S. A. 2016. TNT version 1.5, including a full implementation of phylogenetic morphometrics. *Cladistics*, **32**, 221–238.

GÓMEZ, R. O. 2016. A new pipid frog from the Upper Cretaceous of Patagonia and early evolution of crown-group Pipidae. *Cretaceous Research*, **62**, 52–64.

GÓMEZ, R. O. and LIRES, A. I. 2019. High ecomorphological diversity among Early Cretaceous frogs from a large subtropical wetland of Iberia. *Comptes Rendus Palevol*, **18**, 711–772.

GÓMEZ, R. O. and PÉREZ-BEN, C. M. 2019. Fossils reveal long-term continuous and parallel innovation in the sacro-caudo-pelvic complex of the highly aquatic pipid frogs. *Frontiers in Earth Science*, **7**, 56.

GÓMEZ, R. O. and TURAZZINI, G. F. 2016. An overview of the ilium of anurans (Lissamphibia, Salientia), with a critical appraisal of the terminology and primary homology of main ilial features. *Journal of Vertebrate Paleontology*, **36**, e1030023.

GÓMEZ, R. O. and TURAZZINI, G. F. 2021a. The fossil record and phylogeny of South American horned frogs (Anura, Ceratophryidae). *Journal of Systematic Palaeontology*, **19**, 91–130.

GÓMEZ, R. O. and TURAZZINI, G. F. 2021b. Data from: The fossil record and phylogeny of South American horned frogs (Anura, Ceratophryidae). *MorphoBank*, P4531. http://dx.doi.org/10.7934/P4531

GÓMEZ, R. O., PÉREZ-BEN, C. M. and STEFANINI, M. I. 2013. Oldest record of *Leptodactylus* Fitzinger, 1826 (Anura, Leptodactylidae), from the early Pliocene of the South American Pampas. *Journal of Vertebrate Paleontology*, **33**, 1321–1327.

GRANT, T., FROST, D. R., CALDWELL, J. P., GAGLIARDO, R., HADDAD, C. F. B., KOK, P. J. R., MEANS, D. B., NOONAN, B. P., SCHARGEL, W. E. and WHEELER, W. 2006. Phylogenetic systematics of dart-poison frogs and their relatives (Amphibia: Athesphatanura: Dendrobatidae). *Bulletin of the American Museum of Natural History*, **299**, 1–262.

GREGORY-WODZICKI, K. M. 2002. A late Miocene subtropical-dry flora from the northern Altiplano, Bolivia. *Palaeogeography, Palaeoclimatology, and Palaeoecology*, **180**, 331–348.

GREGORY-WODZICKI, K. M., MCINTOSH, W. C. and VELASQUEZ, K. 1998. Climatic and tectonic implications of the late Miocene Jakokkota flora, Bolivian Altiplano. *Journal of South American Earth Sciences*, **11**, 533–560.

GUEVARA, J. P., LARA, F. S., ALARCÓN-MUÑOZ, J., BULDRINI, K. E., SOTO-ACUÑA, S. and RUBILAR-ROGERS, D. 2022. The first fossil toad (Anura: Bufonidae) from the Cura-Mallín Formation (Río Pedregoso Member, middle Miocene) of Lonquimay, Araucania Region, Central Chile. *Journal of South American Earth Sciences*, **115**, 103753.

HIME, P. M., LEMMON, A. R., LEMMON, E. C. M., PRENDINI, E., BROWN, J. M., THOMSON, R. C., KRATOVIL, J. D., NOONAN, B. P., PYRON, R. A., PELOSO, P. L. and KORTYNA, M. L. 2021. Phylogenomics reveals ancient gene tree discordance in the amphibian tree of life. *Systematic Biology*, **70**, 49–66.

HOFFSTETTER, R., MARTINEZ, C. M. and TOMASI, P. 1972. Nouveaux gisements de Mammiferés néogènes dans les couches rouges de l'Altiplano bolivien. *Comptes rendus de l'Académie des sciences*, **275**, 739–742.

HUELSENBECK, J. P., NIELSEN, R. and BOLLBACK, J.P. 2003. Stochastic mapping of morphological characters. *Systematic Biology*, **52**, 131–58.

HUTCHISON, V. H., HAINES, H. B. and ENGBRETSON, G. 1976. Aquatic life at high altitude: respiratory adaptations in the Lake Titicaca frog, *Telmatobius culeus*. *Respiration Physiology*, **27**, 115–129.

HUTTER, C. R., LAMBERT, S. M. and WIENS, J. J. 2017. Rapid diversification and time explain amphibian richness at different scales in the Tropical Andes, Earth's most biodiverse hotspot. *The American Naturalist*, **190**, 828–843.

IUCN SSC Amphibian Specialist Group. 2020. *Telmatobius culeus.* Errata version published in 2020 (03/06/2023). The IUCN Red List of Threatened Species 2020: e.T57334A178948447. https://dx.doi.org/10.2305/IUCN.UK.2020-2.RLTS.T57334A178948447.en

JOHNSTON, P. 2011 Cranial muscles of the anurans *Leiopelma hochstetteri* and *Ascaphus truei* and the homologies of the mandibular adductors in Lissamphibia and other gnathostomes. *Journal of Morphology*, **272**, 1492–1512.

KIKINIS, R., PIEPER, S. D. and VOSBURGH, K. G. 2014. 3D Slicer: a platform for subjectspecific image analysis, visualization, and clinical support. 277–289. *In* Jolesz, F. A. (ed). *Intraoperative Imaging and Image-Guided Therapy*. Springer, New York, 893 pp.

LAURENT, R. F. and LAVILLA, E. O. 1986. Redescripción de *Telmatobius hauthali* Koslowsky (Anura: Leptodactylidae) y descripción de una nueva especie del mismo género. *Cuadernos de Herpetología*, **2**, 1–24.

LAVILLA, E. O. and LAURENT, R. F. 1988. Deux nouvelles espèces du genre *Telmatobius* (Anura : Leptodactylidae) en provenance de El Moreno (Province de Jujuy, Argentine). *Alytes*, **7**, 77–89.

LAVILLA, E. O. and BARRIONUEVO, J. S. 2005. El género *Telmatobius* en la República Argentina: una síntesis. 115–165. *In* Lavilla, E. O. and De la Riva, I. (eds). *Studies on the Andean Frogs of the Genera* Telmatobius *and* Batrachophrynus *(Anura: Leptodactylidae)*. *Monografías de Herpetología 7*. Asociación Herpetológica Española, Valencia, 349 pp.

LAVILLA, E. O. and ERGUETA SANDOVAL, P. 1995. Una nueva especie de *Telmatobius* (Anura: Leptodactylidae) del Sudoeste de Bolivia. *Ecología en Bolivia*, **24**, 91–101.

LAVILLA, E. O. and ERGUETA SANDOVAL, P. 1999. A new Bolivian species of the genus *Telmatobius* (Anura: Leptodactylidae) with a humeral spine. *Amphibia-Reptilia*, **20**, 55-64.

LIRES, A. I., SOTO, I. and GÓMEZ, R. O. 2016. Walk before you jump: new insights on frog locomotion from the oldest known salientian. *Palaeobiology*, **42**, 612–623.

LOBO GAVIOLA, F. J. 1989. Osteología Comparada de Tres Especies de *Telmatobius* (Anura: Leptodactylidae) de la Provincia de Tucumán (Argentina). Unpublished licenciate thesis, Facultad de Ciencias Naturales, Universidad Nacional de Tucumán, Tucumán, Argentina, 65 pp.

LYNCH, J. D. 1971. Evolutionary relationships, osteology, and zoogeography of leptodactyloid frogs. *University of Kansas Museum of Natural History Miscellaneous Publications*, **53**, 1–238.

LYNCH, J. D. 1978. A re-assessment of the telmatobiine leptodactylid frogs of Patagonia. *Occasional Papers of the Museum of Natural History, University of Kansas*, **72**, 1– 57.

LYNCH, J. D. 1986. Origins of the high Andean herpetological fauna. 478–499. *In* Vuilleumier, F. and Monasterio, M. (eds). *High Altitude Tropical Biogeography*. Oxford University Press, New York, 649 pp.

MADDISON, W. P. and MADDISON, D. R. 2018. Mesquite: a modular system for evolutionary analysis. Version 3.6. http://www.mesquiteproject.org

MAGLIA, A. M., PUGENER, L. A. and MUELLER, J. M. 2007. Skeletal morphology and postmetamorphic ontogeny of *Acris crepitans* (Anura: Hylidae): a case of miniaturization in frogs. *Journal of Morphology*, **268**, 194–223.

MARJANOVIĆ, D. and LAURIN, M. 2008. Assessing confidence intervals for stratigraphic ranges of higher taxa: the case of Lissamphibia. *Acta Palaeontologica Polonica*, **53**, 413–432.

MARTÍNEZ, C., JARAMILLO, C., CORREA-METRÍO, A., CREPET, W., MORENO, J. E., ALIAGA, A., MORENO, F., IBAÑEZ-MEJIA and M., BUSH, M. B. 2020. Neogene precipitation, vegetation, and elevation history of the Central Andean Plateau. *Science Advances*, **6**, 1–9.

MOEN, D. S., MORLON, H. and WIENS, J. J. 2016. Testing convergence versus history: convergence dominates phenotypic evolution for over 150 Million Years in frogs. *Systematic Biology*, **65**, 146–160.

MUELLER, R. L. 2006. Evolutionary rates, divergence dates, and the performance of mitochondrial genes in Bayesian phylogenetic analysis. *Systematic Biology*, **55**, 289–300.

MUÑOZ-SARAVIA, A. 2018. Foraging strategies and ecology of Titicaca water frog (*Telmatobius culeus*). Unpublished PhD thesis, Ghent University, Belgium, 224 pp.

MUÑOZ-SARAVIA, A., CALLAPA, G. and JANSSENS, G. P. 2018. Temperature exposure and possible thermoregulation strategies in the Titicaca water frog *Telmatobius culeus*, a fully aquatic frog of the High Andes. *Endangered Species Research*, **37**, 91–103.

PARHAM, J. F., DONOGHUE, P. C., BELL, C. J., CALWAY, T. D., HEAD, J. J., HOLROYD, P. A., INOUE, J. G., IRMIS, R. B., JOYCE, W. G., KSEPKA, D. T., PATANÉ, J. S. L., SMITH, N. D., TARVER, J. E., VAN TUINEN, M., YANG, Z., ANGIELCZYK, K. D., GREENWOOD, J. M., HIPSLEY, C. A., JACOBS, L., MAKOVICKY, P. J., MÜLLER, J., SMITH, K. T., THEODOR, J. M., WARNOCK, R. C. M. and BENTON, M. J. 2012. Best practices for justifying fossil calibrations. *Systematic Biology*, **61**, 346–359.

PÉREZ-BEN, C. M., TURAZZINI, G. F. and GÓMEZ, R. O. 2019. A Last Glacial anuran assemblage from the inland Pampas of South America provides insights into climate and environments during Marine Isotope Stage 3. *Journal of Vertebrate Paleontology*, **39**, e1627365.

PONSSA, M. L. 2008. Cladistic analysis and osteological descriptions of the frog species in the *Leptodactylus fuscus* species group (Anura, Leptodactylidae). *Journal of Zoological Systematics and Evolutionary Research*, **46**, 249–266.

PRÁMPARO, M. B., ANTOINE, P-O, MARIVAUX, L., ANDRADE FLORES, R., FERNÁNDEZ-MONESCILLO, M., BOSCAINI, A., MAMANI QUISPE, B., FAUQUETTE, S., BONNET, C., MÜNCH, P. and PUJOS, F. 2022. Occurrence of *Cyclusphaera scabrata* in Achiri (late middle-early late Miocene?, Bolivian Altiplano): paleogeographical implication. *Journal of South American Earth Sciences*, **119**, 103990.

PUJOS, F., ANTOINE, P.-O., MAMANI QUISPE, B., ABELLO, A. and ANDRADE FLORES, R. 2012. The Miocene vertebrate faunas of Achiri, Bolivia. *Journal of Vertebrate Paleontology*, **32** (Supp. to 3), 159.

PYRON, R. A. 2014. Biogeographic analysis reveals ancient continental vicariance and recent oceanic dispersal in amphibians. *Systematic Biology*, **63**, 779–797.

R CORE TEAM 2013. R: a language and environment for statistical computing. R Foundation for Statistical Computing. https://www.R-project.org

REIG, O. A. 1958. Proposiciones para una nueva macrosistemática de los anuros. Nota preliminar. *Physis*, **21**, 109–118.

REIG, O. A. and CEI, J. M. 1963. Elucidación monfológico-estadística de las entidades del género *Lepidobatrachus* Budget (Anura, Ceratophryinidae) con consideraciones sobre la extensión del distrito chaqueño del dominio zoogeográfico subtropical. *Physis*, **67**, 181–204.

REVELL, L. J. 2012. phytools: a R package for phylogenetic comparative biology (and other things). *Methods in Ecology and Evolution*, **3**, 217–223.

ROELANTS, K., GOWER, D. J., WILKINSON, M., LOADER, S. P., BIJU, S. D., GUILLAUME, K., MORIAU, L. and BOSSUYT, F. 2007. Global patterns of diversification in the history of modern amphibians. *Proceedings of the National Academy of Sciences of the United States of America*, **104**, 887–892.

ROTHSCHILD, B. M., SCHULTZE, H. P. AND PELLEGRINI, R. 2012. *Herpetological Osteopathology: Annotated Bibliography of Amphibians and Reptiles*. Springer Science and Business Media, Berlin/Heidelberg, 450 pp.

SÁEZ, P. A., FIBLA, P., CORREA, C., SALLABERRY, M., SALINAS, H., VELOSO, A., MELLA, J., ITURRA, P. and MÉNDEZ, M. 2014. A new endemic lineage of the Andean frog genus *Telmatobius* (Anura, Telmatobiidae) from the western slopes of the central Andes. *Zoological Journal of the Linnean Society*, **171**, 769–782.

SÁEZ, P. A., ZÚÑIGA-REINOSO, Á., FIBLA, P., CRUZ-JOFRÉ, F., AGUILAR, C., APARICIO, J., CUSI, J. C., OTÁLORA, K. AND MÉNDEZ, M. A. 2022. Phylogeny of *Telmatobius marmoratus* complex (Anura, Telmatobiidae) reveals high cryptic diversity in the Andean Altiplano. *Molecular Phylogenetics and Evolution*, **176**, 107594.

SAINT-ANDRÉ, P.-A. 1993. *Hoffstetterius imperator* n. g., n. sp. du Miocène supérieur de l'Altiplano bolivien et le statut des Dinotoxodontinés (Mammalia, Notoungulata). *Comptes Rendu de l'Académie des Sciences de Paris*, **316**, 539–545.

SCHINDELIN, J., ARGANDA-CARRERAS, I., FRISE, E., KAYNIG, V., LONGAIR, M., PIETZSCH, T., PREIBISCH, S., RUEDEN, C., SAALFELD, S., SCHMID, B., TINEVEZ, J. Y., WHITE, D. J., HARTENSTEIN, V., ELICEIRI, K., TOMANCAK, P. and CARDONA, A. 2012. Fiji: An open-source platform for biological-image analysis. *Nature Methods*, **9**, 676–682.

SEIMON, T. A., SEIMON, A., DASZAK, P., HALLOY, S. R. P., SCHLOEGEL, L. M., AGUILAR, C. A., SOWELL, P., HYATT, A. D., KONECKY, B. and SIMMONS, J. E. 2007. Upward range extension of Andean anurans and chytridiomycosis to extreme elevations in response to tropical deglaciation. *Global Change Biology*, **13**, 288–299.

SINSCH, U., HEIN, K. and GLUMP, B. 2005. Reassessment of central Peruvian Telmatobiidae (genera *Batrachophrynus* and *Telmatobius*): osteology, palmar morphology and skin histology. 239–260. *In* Lavilla, E. O. and De la Riva, I. (eds). *Studies on the Andean Frogs of the Genera* Telmatobius *and* Batrachophrynus *(Anura: Leptodactylidae)*. *Monografías de Herpetología 7*. Asociación Herpetológica Española, Valencia, 349 pp.

SIRVAS-CARRANZA, F. and TORRES, E. 1966. Consideraciones geológicas de la zona noroeste de la Provincia Pacajes del depto. La Paz. *Boletín del Instituto Boliviano del Petróleo*, **66**, 54–64.

SOKOL, O. M. 1969. Feeding in the pipid frog *Hymenochirus boettgeri* (Tornier). *Herpetologica*, **25**, 9–24.

STREICHER, J. W., MILLER, E. C., GUERRERO, P. C., CORREA, C., ORTIZ, J. C., CRAWFORD, A. J., PIEF, M. R. and WIENS, J. J. 2018. Evaluating methods for phylogenomic analyses, and a new phylogeny for a major frog clade (Hyloidea) based on 2214 loci. *Molecular Phylogenetics and Evolution*, **119**, 128–143.

SUAZO LARA, F. and GÓMEZ, R. O. 2022. In the shadow of dinosaurs: Late Cretaceous frogs are distinct components of a widespread tetrapod assemblage across Argentinean and Chilean Patagonia. *Cretaceous Research*, **131**, 105085.

TRUEB, L. 1979. Leptodactylid frogs of the genus *Telmatobius* in Ecuador with the description of a new species. *Copeia*, **1979**, 714–733.

TURAZZINI, G. F. and GÓMEZ, R. O. 2023a. A new old Budgett frog: an articulated skeleton of an early Pliocene *Lepidobatrachus* (Anura, Ceratophryidae) from western Argentina. *Journal Vertebrate Paleontology*, **42**, e2207092.

TURAZZINI, G. F. and GÓMEZ, R. O. 2023b. Comparative osteology of paradoxical frogs (Hylidae: Pseudae) with comments on diagnostic features, evolutionary trends and potential aquatic adaptations. *Zoologischer Anzeiger*, **43**, 47–70.

TURAZZINI, G. F., GÓMEZ, R. O. and TAGLIORETTI, M. L. 2014. El inusual hallazgo de una asociación diversa de anuros en Yacimiento Constitución (Pleistoceno Tardío, Mar del Plata) con el primer registro fósil de *Pseudis* Wagler (Hylidae, Anura). *Ameghiniana*, Supplement, **51**, 22.

TURAZZINI, G. F., TAGLIORETTI, M. L. and GÓMEZ, R. O. 2016. First fossil record of the South American frog genus *Odontophrynus* Reinhardt and Lütken, 1862 (Anura, Neobatrachia). *Journal Vertebrate Paleontology*, **36**, e1228657.

VELLARD, J. 1951. Estudios sobre batracios andinos. I. El grupo *Telmatobius* y formas afines. *Memorias del Museo de Historia Natural 'Javier Prado'*, **1**, 1–89.

VILLARROEL, C. 1974. Les mésothérinés (Notoungulata, Mammalia) du Pliocène de Bolivie leurs rapports avec ceux d'Argentine. *Annales de Paléntologie*, **60**, 245–281.

WEBER, R. E. 2014. Enthalpic consequences of reduced chloride binding in Andean frog (*Telmatobius peruvianus*) hemoglobin. *Journal of Comparative Physiology B*, **184**, 613–621.

WIEGMANN, A. F. A. 1834. Amphibien. 433–522. *In* Meyen, F. J. F. (ed). *Reise um die Erde ausfeführt auf dem Königlich Preussischen Seehandlungs-Schiffe Prinzes Louise, comandiert von Captain W. Wendt, in den Jahren 1830, 1831 und 1832 von Dr. F. J. F. Meyen. Dritter Theil. Zoologisher Bericht*. Sanderschen Buchhandlung (C. W. Eichhoff), Berlin, 493 pp.

WIENS, J. J. 1993. Systematics of the leptodactylid frog genus *Telmatobius* in the Andes of northern Peru. *Occasional Papers of the Museum of Natural History, University of Kansas*, **162**, 1–76.

FIGURE CAPTIONS

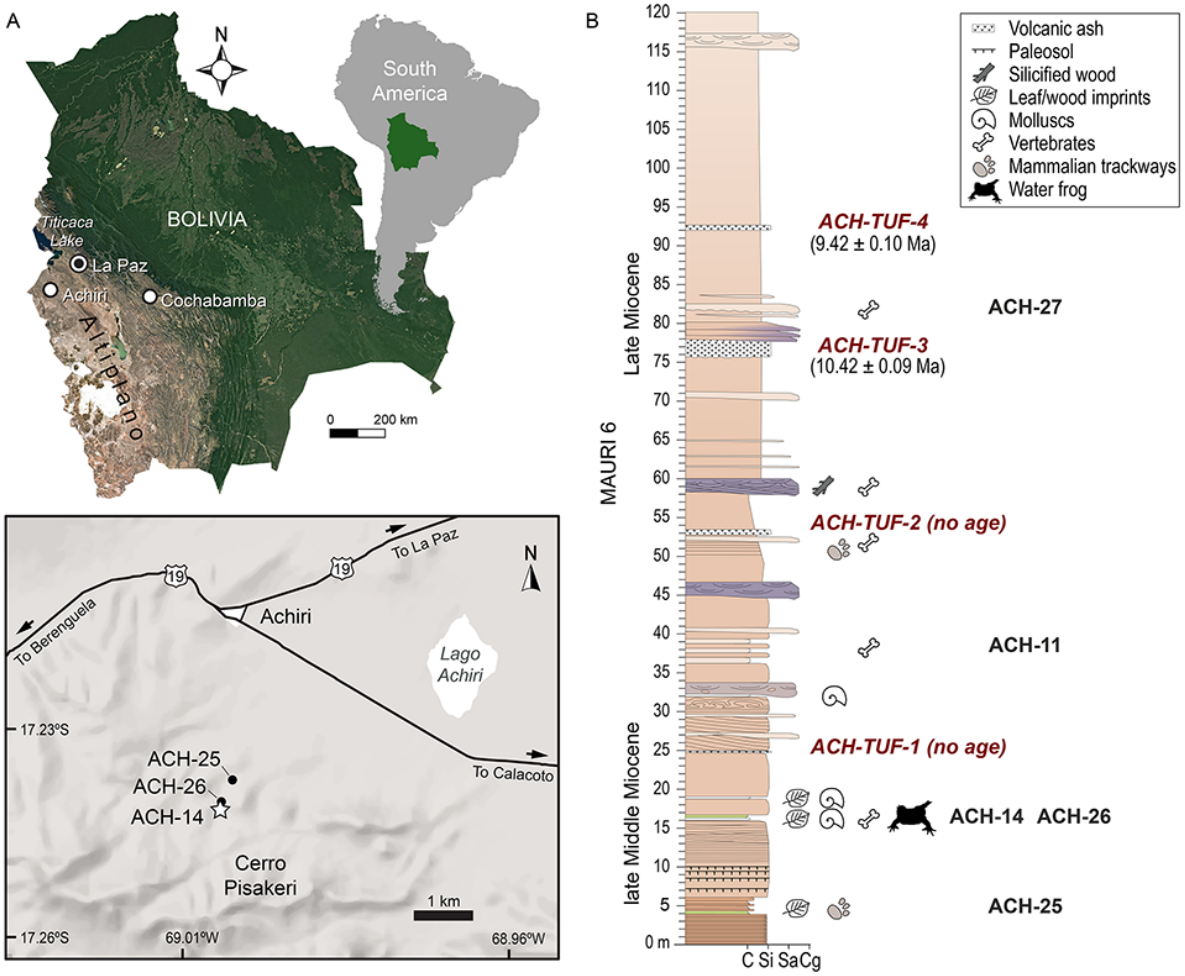

FIG. 1. A, location map of Achiri village, Pacajes Province, La Paz Department, Bolivia, marking the type locus ACH-14 (star) and loci ACH-25 and ACH-26 (black dots) in the region of Cerro Pisakeri (Maps data: Google Earth, SIO, NOAA, US Navy, NGA, GEBCO, Image Landsat/Copernicus). B, stratigraphic column of the Member 6 of Mauri Fm. at Cerro Pisakeri (late Middle–early Late Miocene), modified from Prámparo et al. (2022), and location of main fossil-yielding (ACH-XX) loci and volcaniclastic levels (ACH-TUF 1–4). All anuran remains described here originate from ACH-14 locus, laterally equivalent to the pollen-bearing ACH-26 locus. *Abbreviations*: C, clay; Cg, conglomerate; Si, siltite; Sa, sand.

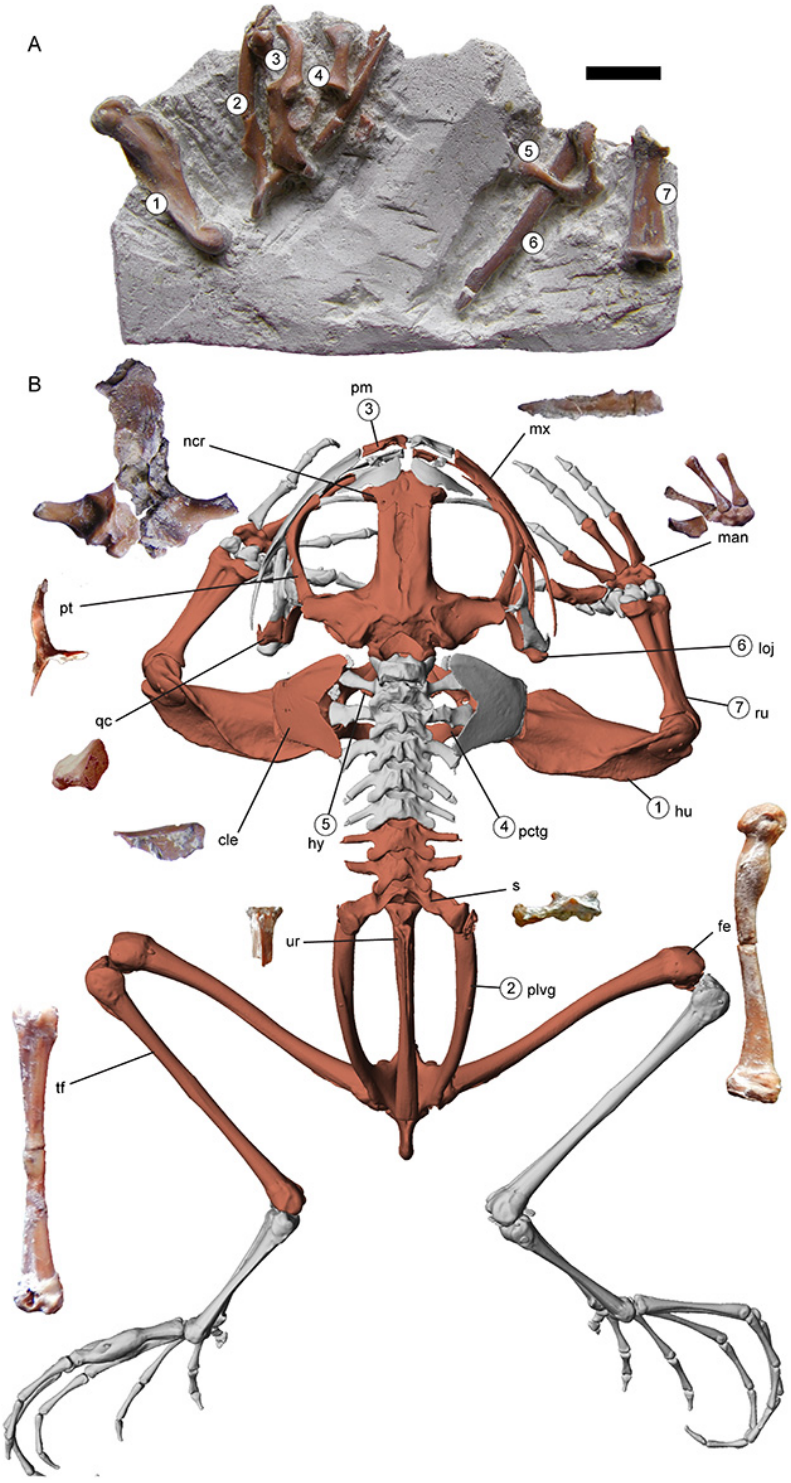

FIG. 2. *Telmatobius achachila* sp. nov., holotype (MNHN-Bol-V 012795). Photographs of the type block and most mechanically isolated fossils representing a single adult male individual. A, type block preserving cranial and postcranial bones (numbered elements are explained in B); B, Isolated bones and restoration of the skeleton in dorsal view (based on *T. thompsoni* UF-H 39734 and scaled to match the size of fossil bones) with the preserved parts highlighted in colour. *Abbreviations*: cle, cleithrum; fe, femur; hu, humerus; hy, hyoid; loj, lower jaw; man, manus; mx, maxilla; ncr, neurocranium; pctg, pectoral girdle; plvg, pelvic girdle; pm, premaxilla; pt, pterygoid; qc, quadrate complex; ru, radio-ulna; s, sacrum; tf, tibiofibula; ur, urostyle. Scale bar represents 1 cm.

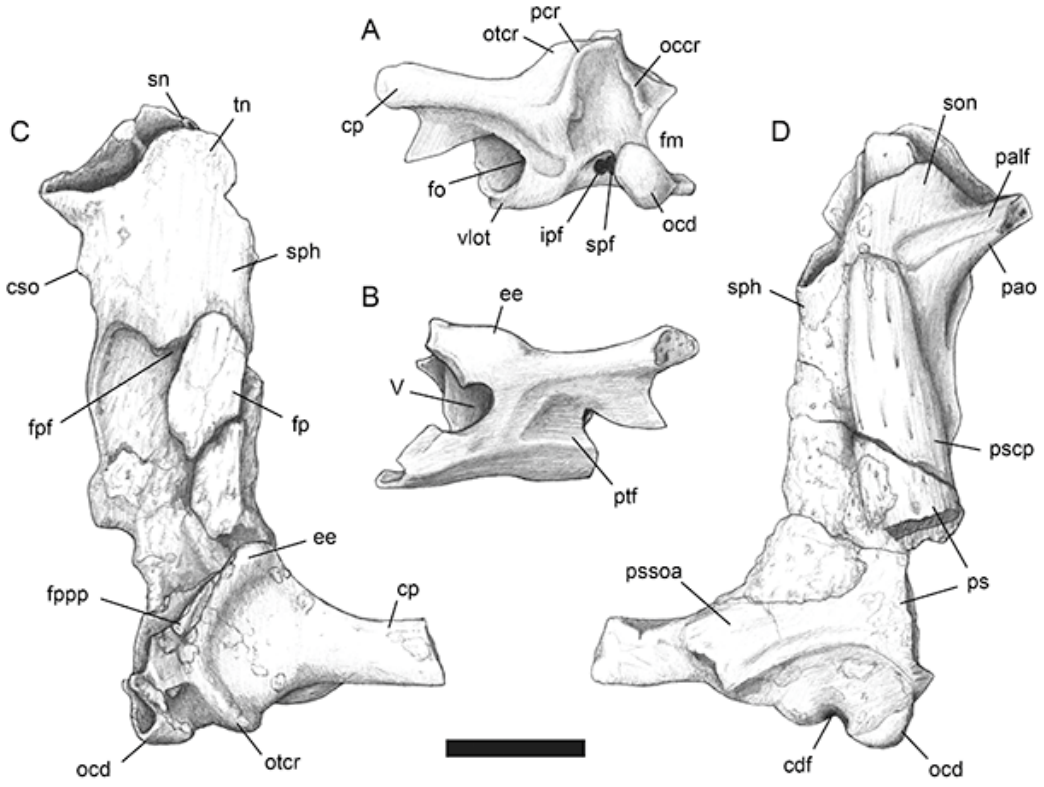

FIG. 3. *Telmatobius achachila* sp. nov., part of the holotype (MNHN-Bol-V 012795). Neurocranium. Left otic capsule in: A, posterior; B, anterior view. Partial neurocranium (including the sphenethmoid and right otic capsule) in: C, dorsal; D, ventral view. *Abbreviations*: V, prootic foramen; cdf, condyloid fossa; cp, crista parotica; cso, crista supraorbitalis; ee, epiotic eminence; fm, foramen magnum; fo, fenestra ovalis; fp, frontoparietal; fpf, frontoparietal fenestra; fppp, paroccipital process of frontoparietal; ipf, inferior perilymphatic foramen; occr, occipital crest; ocd, occipital condyle; otcr, otic crest; palf, palatine facet; pao, planum antorbitale; pcr, posterior crest parallel to otic crest; ps, parasphenoid; pscp, cultriform process of parasphenoid; pssoa, subotic alae of parasphenoid; ptf, pterygoid facet; sn, septum nasi; son, solum nasi; spf, superior perilymphatic foramen; sph, sphenethmoid; tn, tectum nasi; vlot, ventrolateral otic ledge. Scale bar represents 5 mm. (Drawings: ROG.)

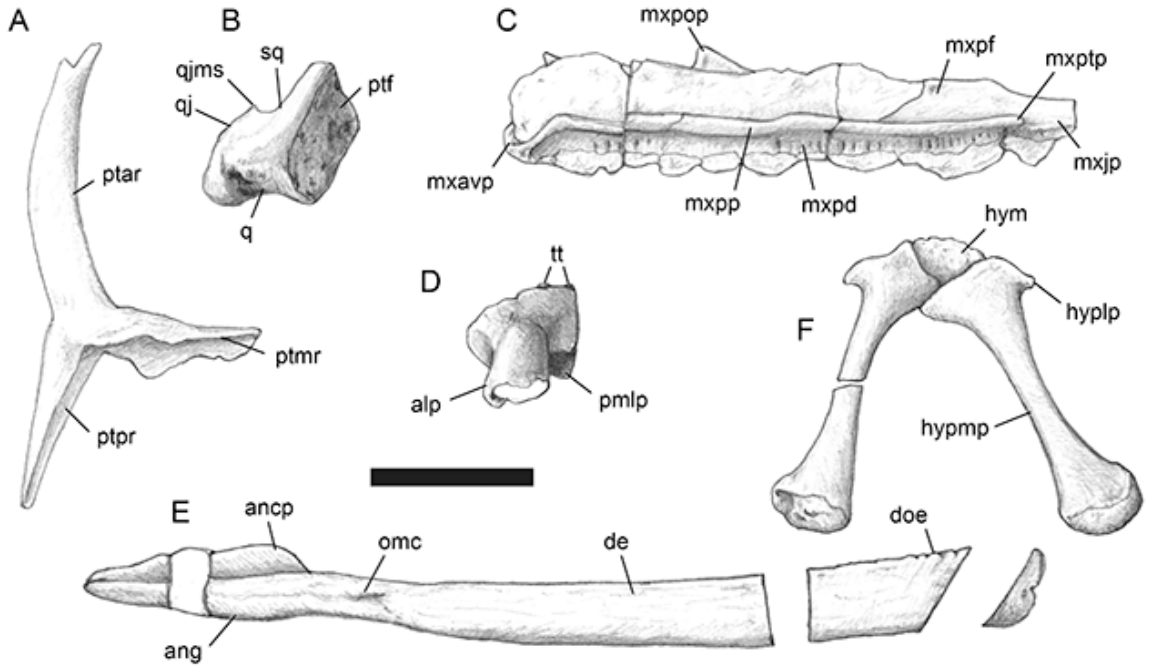

FIG. 4. *Telmatobius achachila* sp. nov., part of the holotype (MNHN-Bol-V 012795). Suspensorium, upper and lower jaws, and hyoid. A, Left pterygoid in dorsal view. B, left quadrate+quadratojugal+fragment of squamosal in dorsomedial view. C, right maxilla in lingual view. D, left premaxilla in dorsal view. E, right lower jaw in labial view (gaps in the anterior part are concealed by the hyoid; see Fig. 2A). F, bony hyoid in ventral view. *Abbreviations*: alp, alary process; ancp, coronoid process of angulosplenial; ang, angulosplenial; de, dentary; doe, oral edge of dentary; hym, hyoid plate mineralisation; hyplp, posterolateral process of hyoid; hypmp, posteromedial process of hyoid; mxavp, anteroventral process of maxilla; mxjp, jugal process of maxilla; mxpd, pars dentalis of maxilla; mxpf, pars facialis of maxilla; mxpop, preorbital process of maxilla; mxpp, pars palatina of maxilla; mxptp, pterygoid process of maxilla; omc, ossified Meckel's cartilage; pmlp, lingual process of premaxilla; ptar, anterior ramus of pterygoid; ptf, facet for the medial ramus of the pterygoid; ptmr, medial ramus of pterygoid; ptpr, posterior ramus of pterygoid; q, pars articularis of the quadrate; qj, quadratojugal; qjms, maxillary spine of quadratojugal; sq, squamosal; tt, teeth. Scale bar represents 5 mm. (Drawings: ROG.)

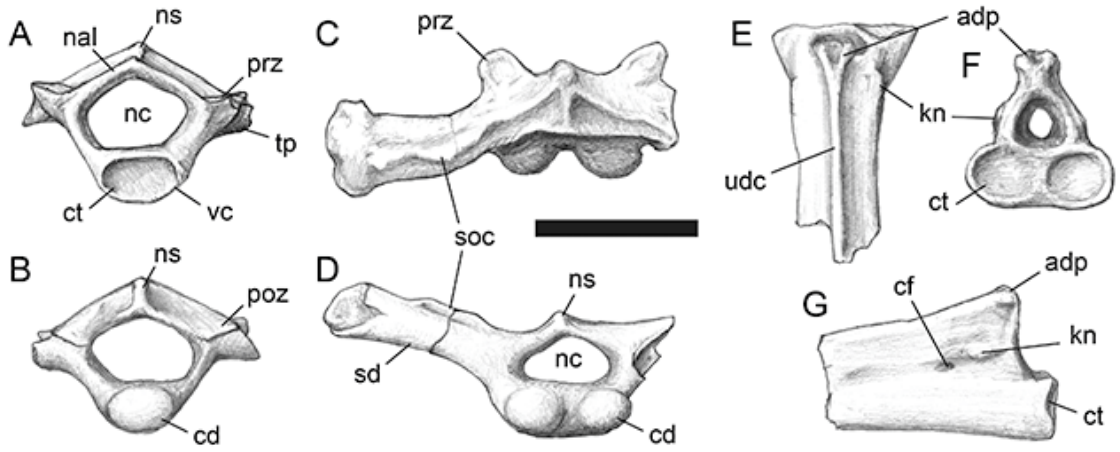

FIG. 5. *Telmatobius achachila* sp. nov., part of the holotype (MNHN-Bol-V 012795). Vertebral column. A, presacral vertebra in anterior view. B, presacral vertebra in posterior view. C, sacral vertebra in dorsal view. D, sacral vertebra in posterior view. E, urostyle in dorsal view. F, urostyle in anterior view. G, urostyle in lateral view. *Abbreviations*: adp, anterodorsal process of urostyle; cd, condyle; cf, coccygeal foramen; ct, cotyle; kn, knob; nal, neural arch lamina; nc, neural canal; ns, neural spine; poz, postzygapophysis; prz, prezygapophysis; sd, sacral diapophysis; soc, sacral oblique crest; tp, transverse process; udc, dorsal crest of urostyle; vc, vertebral centra. Scale bar represents 2 mm. (Drawings: ROG.)

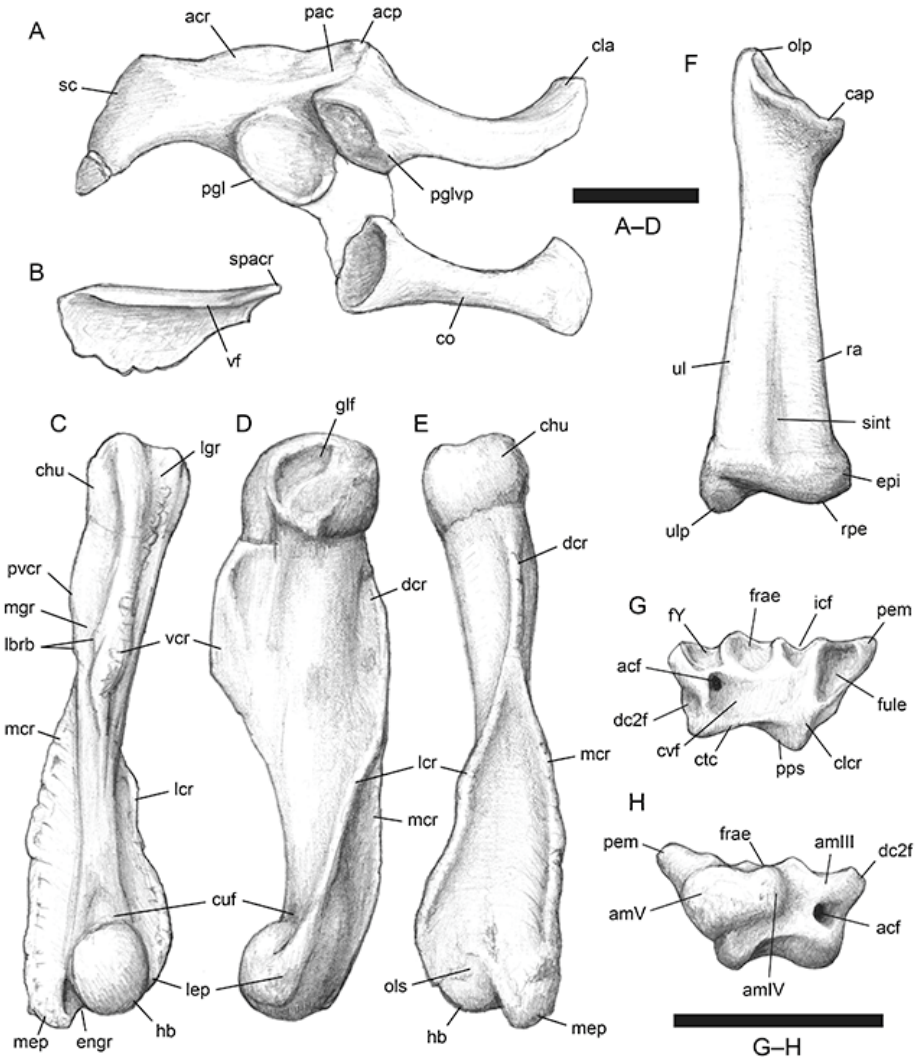

FIG. 6. *Telmatobius achachila* sp. nov., part of the holotype (MNHN-Bol-V 012795). Pectoral girdle and forelimbs. A, right scapula, clavicle, and coracoid in glenoid view (as articulated in the main block). B, left cleithrum in ventral (internal) view. C, left humerus in ventral view. D, left humerus in lateral view. E, left humerus in dorsal view. F, right radio-ulna in lateral view. G, right Distal Carpal 5-4-3 in proximal/volar view. G, right Distal Carpal 5-4-3 in distal view. *Abbreviations*: acf, anterior carpal foramen; acp, acromial process; acr, anterior crest of scapula; amIII, articular surface for metacarpal III; amIV, articular surface for metacarpal IV; amV, articular surface for metacarpal V; cap, capitulum; chu, caput humeri; cla, clavicle; clcr, continuation of longitudinal crest; co, coracoid; ctc, carpal transverse crest; cuf, cubital fossa; cvf, carpal volar fovea; dc2f, facet for Distal Carpal 2; engr, entepicondylar groove; epi, epiphysis; frae, facet for radiale; fule, facet for ulnare; fY, facet for Element Y; glf, glenoid fovea; hb, humeral ball; icf, intercarpal foramen; lbrb, ligamentous bridge bony bases; lcr, lateral crest; lep, lateral epicondyle; lgr, longitudinal groove; mcr, medial crest; mep, medial epicondyle; mgr, medial groove for the tendon of the coracoradialis muscle; olp, olecranean process; ols, olecranean scar; pac, pars acromialis; pem, process for extensor muscles; pgl, pars glenoidalis; pglvp, paraglenoid ventral protuberance; pps, palmar protruding surface; pvcr, paraventral crest; ra, radius; rpe, radial portion of epiphysis; sc, scapula; sint, sulcus intermedius; spacr, spina acromialis; ul, ulna; ulp, ulnar protuberance; vcr, ventral crest; vf, ventral fold. Scale bar represents 5 mm. (Drawings: ROG.)

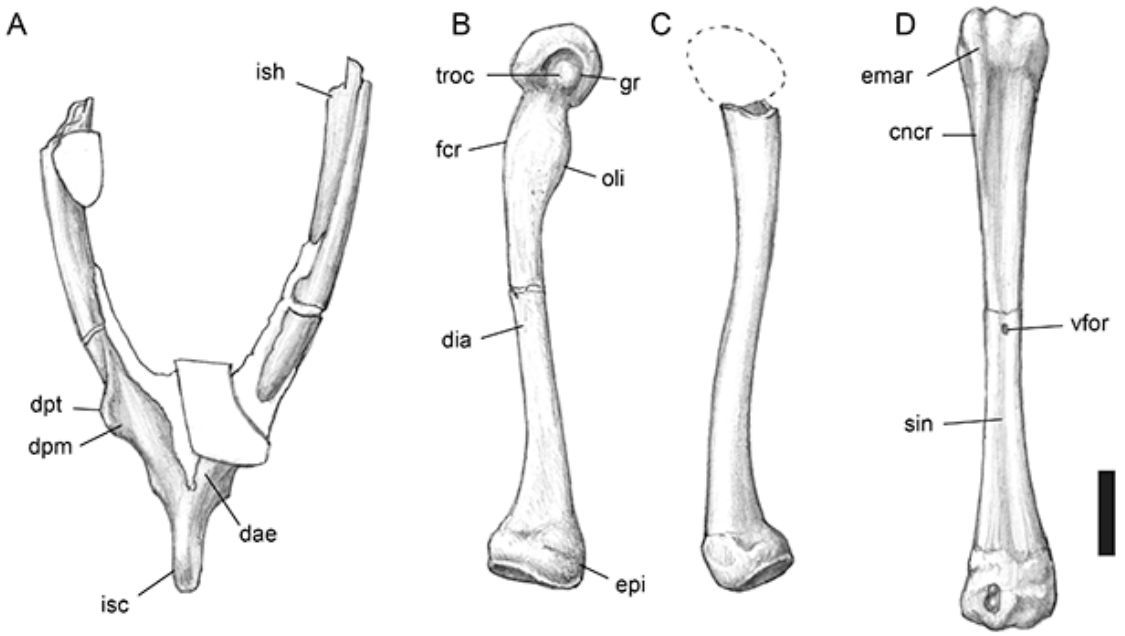

FIG. 7. *Telmatobius achachila* sp. nov., part of the holotype (MNHN-Bol-V 012795). Pelvic girdle and hind limbs. A, pelvic girdle in dorsal view (white areas denoting matrix or overlying bones). B, right pathologic femur in posterolateral view. C, left femur in posterolateral view (dash line depict the unpreserved epiphysis). D, left tibiofibula in ventral view. *Abbreviations*: cncr, cnemial crest; dae, dorsal acetabular expansion; dia, diaphysis; dpm, dorsal prominence; dpt, dorsal protuberance; emar, eminentia arquata; epi, epiphysis; fcr, femoral crest; isc, ischium; ish, iliac shaft; oli, osteomyelitis-like inflammation; sin, sulcus intermedius; troc, trochanter; vfor, ventral foramen. Scale bar represents 5 mm. (Drawings: ROG.)

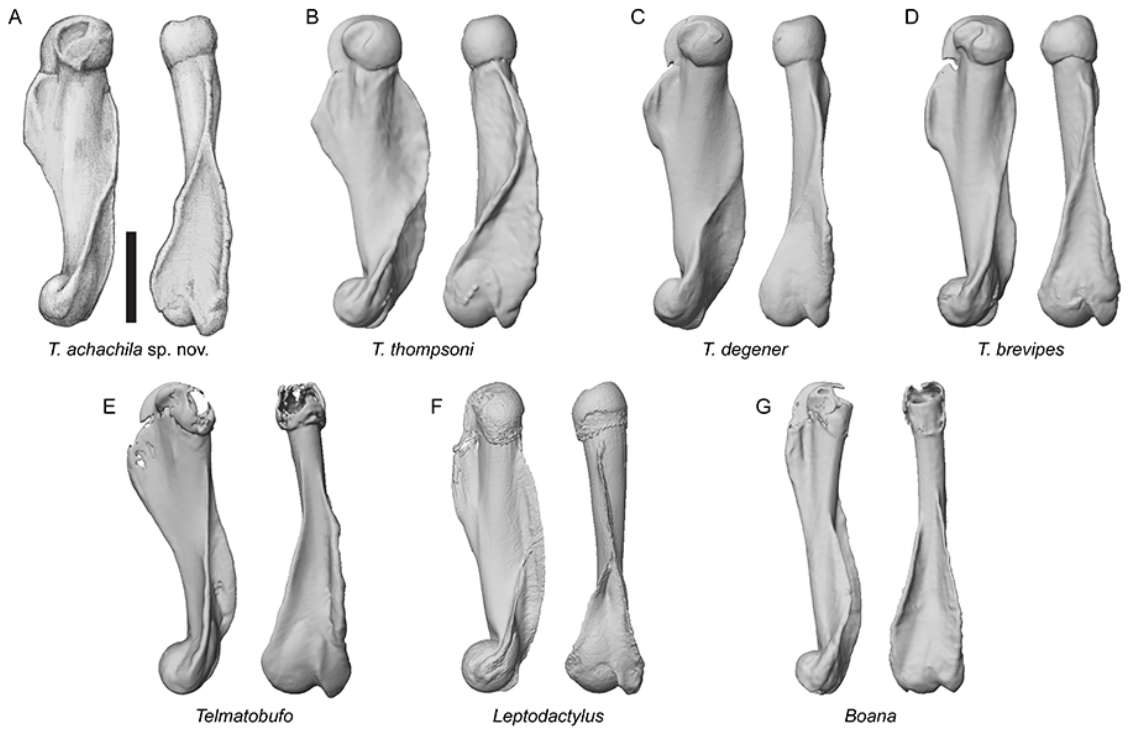

FIG. 8. Left humerus of *Telmatobius achachila* sp. nov. and different extant anurans with enlarged lateral and medial crests in males, in lateral and dorsal views. A, *Telmatobius achachila* sp. nov., holotype (MNHN-Bol-V 012795). B, *Telmatobius thompsoni* (UF-H 39734). C, *Telmatobius degener* (UF-H 39736). D, *Telmatobius brevipes* (UF-H 39760). E, *Telmatobufo bullocki* (KU 161438). F, *Leptodactylus pentadactylus* (UF-H 103788). G, *Boana heilprini* (UF-H 57613). Humeri are scaled according to their total length. Scale bars represent 2 mm.

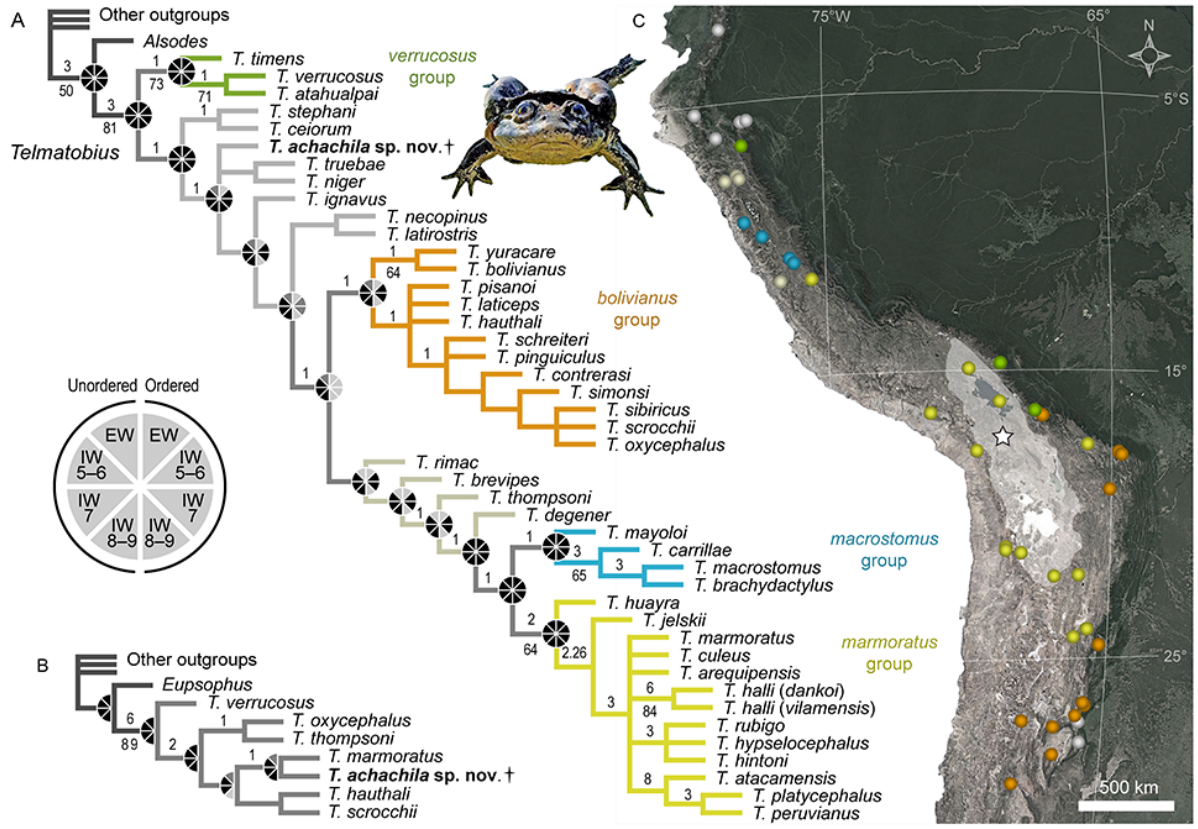

FIG. 9. Phylogenetic relationships of *Telmatobius achachila* sp. nov., summarised on the topologies obtained under implied weights (k = 7) with multistate characters unordered. A, Strict consensus of the four MPTs from the analysis of dataset B17, with the species groups mentioned in the text in colour. B, Single MPT from the analysis of dataset GT21. Bremer support (above 1) and jackknife absolute frequencies (above 50%) are indicated above and below branches, respectively. Pie charts indicate recovery of nodes under different analytical conditions (EW, equal weights; IW, implied weights, with different values of k indicated): solid black is recovered, dark grey is not recovered, but consistent, and light grey is contradicted (note that dataset GT21 was analysed only with characters unordered). Relationships of outgroup taxa are shown in Appendix S4. C, Distribution of sampled species of *Telmatobius* (type localities indicated on map), using the same colour scheme as in the tree in A and indicating the provenance of *T. achachila* (star, Achiri) and current extension of the Altiplano (shaded). (Map data: Google Earth, SIO, NOAA, US Navy, NGA, GEBCO, Image Landsat/Copernicus. Frog drawing: ROG.)

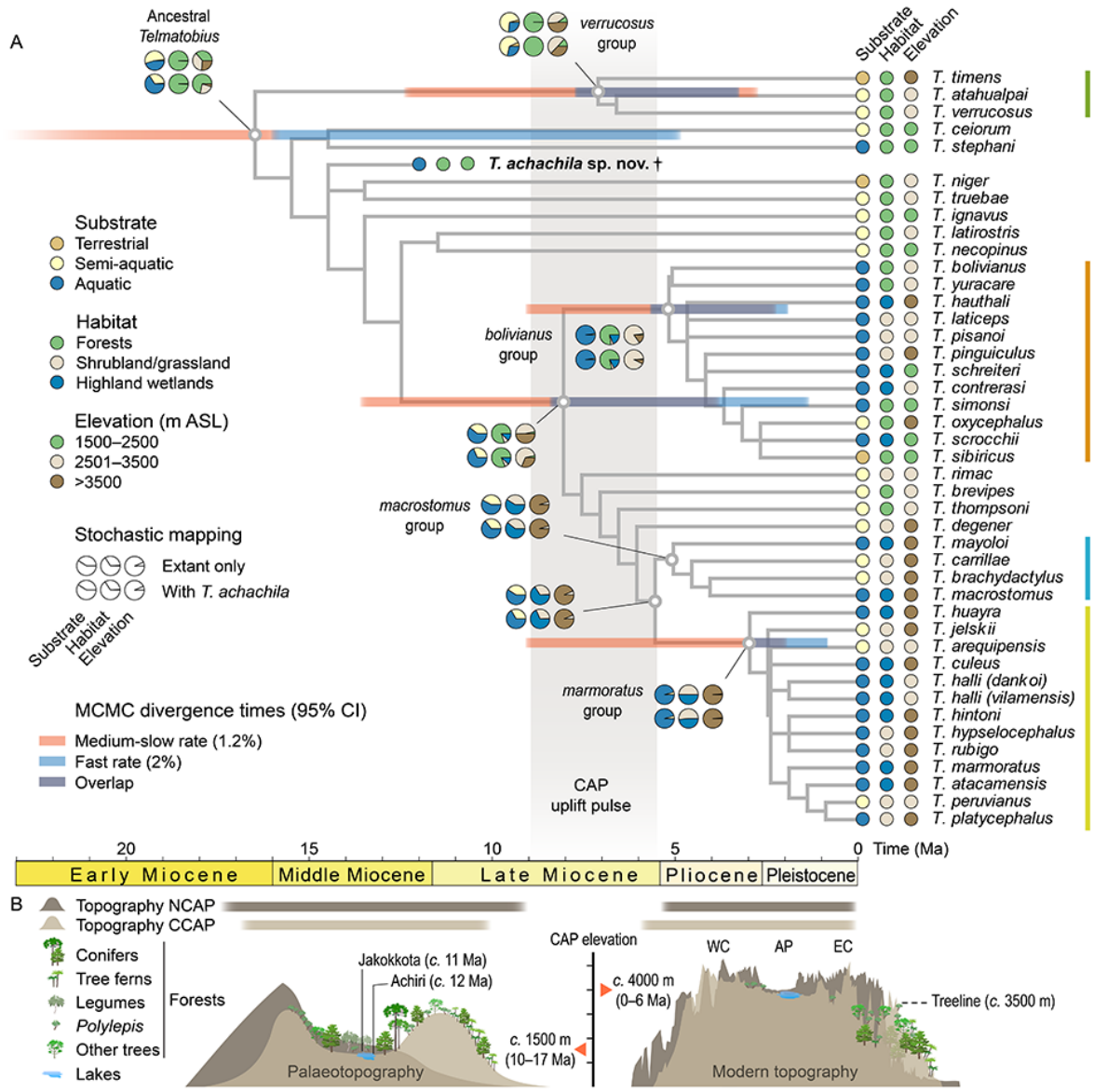

FIG. 10. Time-adjusted evolution of *Telmatobius* and the Altiplano. A, Time-tree based on the strict consensus of Figure 9A, highlighting the age of *Telmatobius achachila* sp. nov. and Bayesian divergence time estimates from De la Riva *et al.* (2010) under two different rates (medium-slow and fast). Pie charts indicate the relative likelihood of ancestral substrate preferences, habitats, and mean elevation ranges, as reconstructed under stochastic character mapping (see text for details). B, Elevation and palaeotopography of the Altiplano over the last 15 Ma based on data reviewed by Garzione *et al.* (2017) and Boschman (2021). *Abbreviations*: ASL, above sea level; CAP, Central Andean Plateau; CCAP, Central 'Central Andean Plateau'; CI, Confidence Interval; EC, Eastern Cordillera; MCMC, Bayesian Markov Chain Monte Carlo; NCAP, Northern 'Central Andean Plateau'; WC, Western Cordillera.

A new early Water Frog (*Telmatobius*) from the Miocene of the Bolivian Altiplano

by RAÚL O. GÓMEZ[1,2]*, TOMÁS VENTURA[1], GUILLERMO F. TURAZZINI[1,2], LAURENT MARIVAUX[3], RUBÉN ANDRADE FLORES[4], ALBERTO BOSCAINI[5,2], MARCOS FERNÁNDEZ-MONESCILLO[6,2], BERNARDINO MAMANI QUISPE[4], MERCEDES B. PRÁMPARO[7,2], SÉVERINE FAUQUETTE[3], CÉLINE MARTIN[8], PHILIPPE MÜNCH[8], FRANÇOIS PUJOS[7,2] *and* PIERRE-OLIVIER ANTOINE[3]*

[1]Departamento de Biodiversidad y Biología Experimental, Facultad de Ciencias Exactas y Naturales, Universidad de Buenos Aires, Ciudad Universitaria, C1428EGA Buenos Aires, Argentina; raulorenciogomez@gmail.com
[2]Consejo Nacional de Investigaciones Científicas y Técnicas (CONICET), Godoy Cruz 2290, C1425FQB Buenos Aires, Argentina
[3]Institut des Sciences de l'Évolution de Montpellier, Univ. Montpellier, CNRS, IRD, F-34095 Montpellier, France; pierre-olivier.antoine@umontpellier.fr
[4]Unidad de Paleontología, Museo Nacional de Historia Natural, Calle 26 s/n, Cota Cota, La Paz, Plurinational State of Bolivia
[5]Instituto de Ecología, Genética y Evolución de Buenos Aires (IEGEBA), Facultad de Ciencias Exactas y Naturales, Universidad de Buenos Aires, Ciudad Universitaria, C1428EGA Buenos Aires, Argentina
[6]Cátedra y Museo de Paleontología, Facultad de Ciencias Exactas, Físicas y Naturales, Universidad Nacional de Córdoba. Vélez Sarsfield 1611, X5016GCA Córdoba, Argentina
[7]Instituto Argentino de Nivología Glaciología y Ciencias Ambientales (IANIGLA), CONICET-UNCUYO-Mendoza, Avda. Ruiz Leal s/n, Parque Gral. San Martín, 5500 Mendoza, Argentina
[8]Géosciences Montpellier, Univ. Montpellier, CNRS, Université des Antilles, F-34095 Montpellier, France

*Corresponding authors

SUPPORTING INFORMATION

Appendix S1. List of **c**omparative materials (see also Table S1).

Abbreviations: CS, cleared and stained; CT, micro CT-scan data on MorphoSource (www.morphosource.org); DS, dry skeleton; LD, data taken from literature.

Institutional abbreviations: AMNH, American Museum of Natural History, New York, USA; CAS, California Academy of Sciences, San Francisco, USA; CBF, Colección Boliviana de Fauna, Museo Nacional de Historia Natural, Academia Nacional de Ciencias de Bolivia, La Paz, Bolivia; CFA, CEBBAD-Fundación Félix de Azara, Buenos Aires, Argentina; CM, Carnegie Museum of Natural History, Pittsburgh, USA; FCEN, Facultad de Ciencias Exactas y Naturales, Universidad de Buenos Aires, Buenos Aires, Argentina; FML, Instituto de Herpetología de la Fundación Miguel Lillo, San Miguel de Tucumán, Argentina; IBIGEO, Instituto de Bio y Geociencias del NOA, Salta, Argentina; KU, Biodiversity Institute, University of Kansas, Lawrence, USA; MACN, Museo Argentino de Ciencias Naturales 'Bernardino Rivadavia', Buenos Aires, Argentina; MCZ, Museum of Comparative Zoology, Harvard University, Cambridge, USA; MLP, Museo de La Plata, La Plata, Argentina; MVZ, Museum of Vertebrate Zoology, University of California, Berkeley, USA; UF, University of

Florida, Florida Museum of Natural History, Gainesville, USA; USNM, National Museum of Natural History, Washington, USA.

Telmatobius. *T. atahualpai* (LD; Aguilar et al. 2012); *T. bolivianus* (LD; Lavilla & Ergueta Sandoval 1999); *T. brevipes*, UF:herp:39760 (CT, ark:/87602/m4/386402) (LD; Wiens 1993); *T. carrillae*, UF:herp:39717 (CT, ark:/87602/m4/M159469); *T. chusmisensis* (LD; Formas et al. 2006); *T. cirrhacelis* (LD; Trueb 1979); *T. culeus*, USNM:Amphibians & Reptiles:281587 (CT, ark:/87602/m4/423141); *T. degener*, UF:herp:39736 (CT, doi:10.17602/M2/M99912) (LD; Wiens 1993); *T. fronteriensis* (LD; Benavides et al. 2002); *T. halli* (LD; Formas et al. 2003); *T. hauthali*, FCEN 320 (DS), FML 3315 (DS); *T. huayra* (LD; Lavilla & Ergueta Sandoval 1995); *T. ignavus* (LD; Wiens 1993); *T. laticeps*, CAS:sua:11270 (CT, ark:/87602/m4/M49875); *T. latirostris* (LD; Wiens 1993); *T. macrostomus*, FCEN 1208-1 (DS); *T. marmoratus*, CAS:herp:152217 (CT, ark:/87602/m4/M49889), KU:kuh 164079, 164080 (DS); *T. mendelsoni* (LD; De la Riva et al. 2012); *T. necopinus* (LD; Wiens 1993); *T. niger* (LD; Trueb 1979); *T. oxycephalus*, FML 2867-II (CS), (LD; Barrionuevo 2013, 2016, 2018); *T. philippii* (LD; Cuevas & Formas 2002); *T. rubigo* (LD; Barrionuevo & Baldo 2009; Barrionuevo 2016, 2018); *T. schreiteri*, FML 541 (DS); *T. scrocchii*, FML 1515 (DS); *T. sibiricus* (LD; De la Riva & Harvey 2003); *T. thompsoni*, UF:herp:39734 (CT, doi:10.17602/M2/M20345) (LD, Wiens 1993); *T. truebae* (LD; Wiens 1993); *T. vellardi* (LD; Trueb 1979); *T. verrucosus*, CBF 5372 (CS); *T. yuracare* (LD; De la Riva 1994).

Alsodidae. *Alsodes nodosus*, CM:herps:68395 (CT, doi:10.17602/M2/M20871), FCEN 722 (DS); *Eupsophus roseus*, AMNH:A-22140 (DS), CM:herps:63926 (CT, doi:10.17602/M2/M21082); *Limnomedusa macroglossa*, CFA-An 138, 192 (DS), CM:herps:55388 (CT, ark:/87602/m4/M116724).

Batrachylidae. *Atelognathus patagonicus*, CAS:herp:141967 (CT, doi:10.17602/M2/M21953); *Batrachyla taeniata*, CAS:herp:85253 (CT, doi:10.17602/M2/M21960); *Hylorina sylvatica*, CAS:herp:141996 (CT, doi:10.17602/M2/M22182), FCEN 304 (DS).

Bufonidae. *Rhinella spinulosa*, MACN-He 45407–45409, 45413 (DS).

Calyptocephalellidae. *Calyptocephalella gayi*, CAS:herp:10082 (CT, doi:10.17602/M2/M24452), FCEN 1433 (DS), MACN-He 45741–45747 (CS & DS); *Telmatobufo bullocki* (as *venustus*), KU:kuh:161438 (CT, doi:10.17602/M2/M42671), KU:kuh:161439 (DS).

Ceratophryidae. *Ceratophrys cranwelli*, CFA-An-73, 104, FCEN 665(2–4), 1015(1–9) (all DS), MCZ:herp:A-35360 (CT, ark:/87602/m4/M70811); *Chacophrys pierottii*, KU:kuh:191932 (CT, doi:10.17602/M2/M37697), MACN-He 47403–47404 (DS & CS); *Lepidobatrachus asper*, FCEN 261 (1), 306, 439 (1, 2), 630 (1–3) (DS), MCZ:herp:A-32777 (CT, ark:/87602/m4/M68634).

Cycloramphidae. *Cycloramphus dubius*, FCEN 758 (DS); *Cycloramphus* (as *Zachaenus*) *parvulus*, CAS:sua:11907 (CT, doi:10.17602/M2/M23008); *Thoropa miliaris*, AMNH:A-20256 (DS), CM:herps:68357 (CT, doi:10.17602/M2/M24444), FCEN 595 (DS).

Hemiphractidae. *Gastrotheca peruana*, UF:herp:65801 (CT, doi:10.17602/M2/M55543).

Hylidae. *Boana pulchella*, CFA-An-273, 276 (DS); *B. heilprini*, UF:herp:57613 (CT, ark:/87602/m4/M162134); *B. riojana*, IBIGEO-A (formerly MCN) 937 (CS); *Bokermannohyla langei* (LD; Faivovich et al. 2009); *Bokermannohyla circumdata*, KU:kuh:91987 (CT, ark:/87602/m4/M162136); *Hyloscirtus armatus* (LD; Duellman et al. 1997); *Phyllomedusa hypochondrialis*, AMNH:A-166281 (CT, ark:/87602/m4/M165653). *Plectrohyla* spp. (LD; Duellman & Campbell 1992); *Pseudis paradoxa*, AMNH:A-71427 (DS), KU:kuh:167676 (DS), UF:herp:71527 (CT, ark:/87602/m4/M163224).

Hylodidae: *Crossodactylus trachystomus*, CM:herps:2662 (CT, ark:/87602/m4/M24014); *Hylodes asper*, CM:herps:45975 (CT, doi:10.17602/M2/M34358), FCEN 762 (DS).

Leptodactylidae: *Leptodactylus fuscus*, FCEN 711, 1704, DS; *L. luctator* (ex *latrans*), CFA-An 128, 131, 185 (DS), FCEN 283, 1931 (DS); *L. pentadactylus*, UF:herp:103788 (CT, ark:/87602/m4/M50004); *Pleurodema cinereum*, FCEN 93 (DS); *P. nebulosa*, CAS:sua:15635 (CT, ark:/87602/m4/M163220).

Microhylidae. *Hamptophryne boliviana*, AMNH:A-115764 (CT, ark:/87602/m4/M154612).

Odontophrynidae. *Odontophrynus americanus*, CFA-An 129, 135 (DS), CM:herps:147828 (CT, doi:10.17602/M2/M25346), FCEN 1096, 1285 (DS); *Proceratophrys boiei*, CM:herps:45986 (CT, doi:10.17602/M2/M29141), FCEN 699 (DS).

Pipidae. *Pipa aspera*, MVZ:herp:247507 (CT, ark:/87602/m4/M165891); *Pipa carvalhoi*, MACN-He 42606–42608 (DS), 42609–42610 (CS), MCZ:herp:a-25737 (CT, doi:10.17602/M2/M12424); *P. parva*, UF:herp:37924 (CT, doi:10.17602/M2/M12417); *P. pipa*, FCEN 1434 (DS); MACN-He 42612 (DS), 42613 (DS); USNM:Amphibians & Reptiles:85032 (CT, ark:/87602/m4/405743); *P. snethlageae*, MACN-He 42611 (DS); MCZ:herp:a-17734 (CT, ark:/87602/m4/M66254). *Xenopus borealis*, CAS:herp:152778 (CT, doi:10.17602/M2/M58062).

Rhinodermatidae. *Rhinoderma darwinii*, UF:herp:62022 (CT, doi:10.17602/M2/M25059).

Strabomantidae. *Pristimantis duellmani*, KU:kuh:179333 (CT, ark:/87602/m4/M61984).

Appendix S2: Character scoring of *Telmatobius achachila*.

T. achachila on dataset B17 from Barrionuevo (2017)

???011[01]?0?0?000???[12]0???1?1?11100011011????20???1?1?0110??????????????????????????????????????

T. achachila on dataset GT21 from Gómez & Turazzini (2021)

00??10?00?0001001020??????1?1000011??100??1?01200000[01]00??0?0??????130??1??????21?????210111?[12]1??????????0100012112?1??2??11??101201[01]1?00????????[01]?0?0?????000????1????00?????10?00?[01]?11?01?1121001O?????101100?0???00?0?1?2??0??????????3?10101??11111111100??10

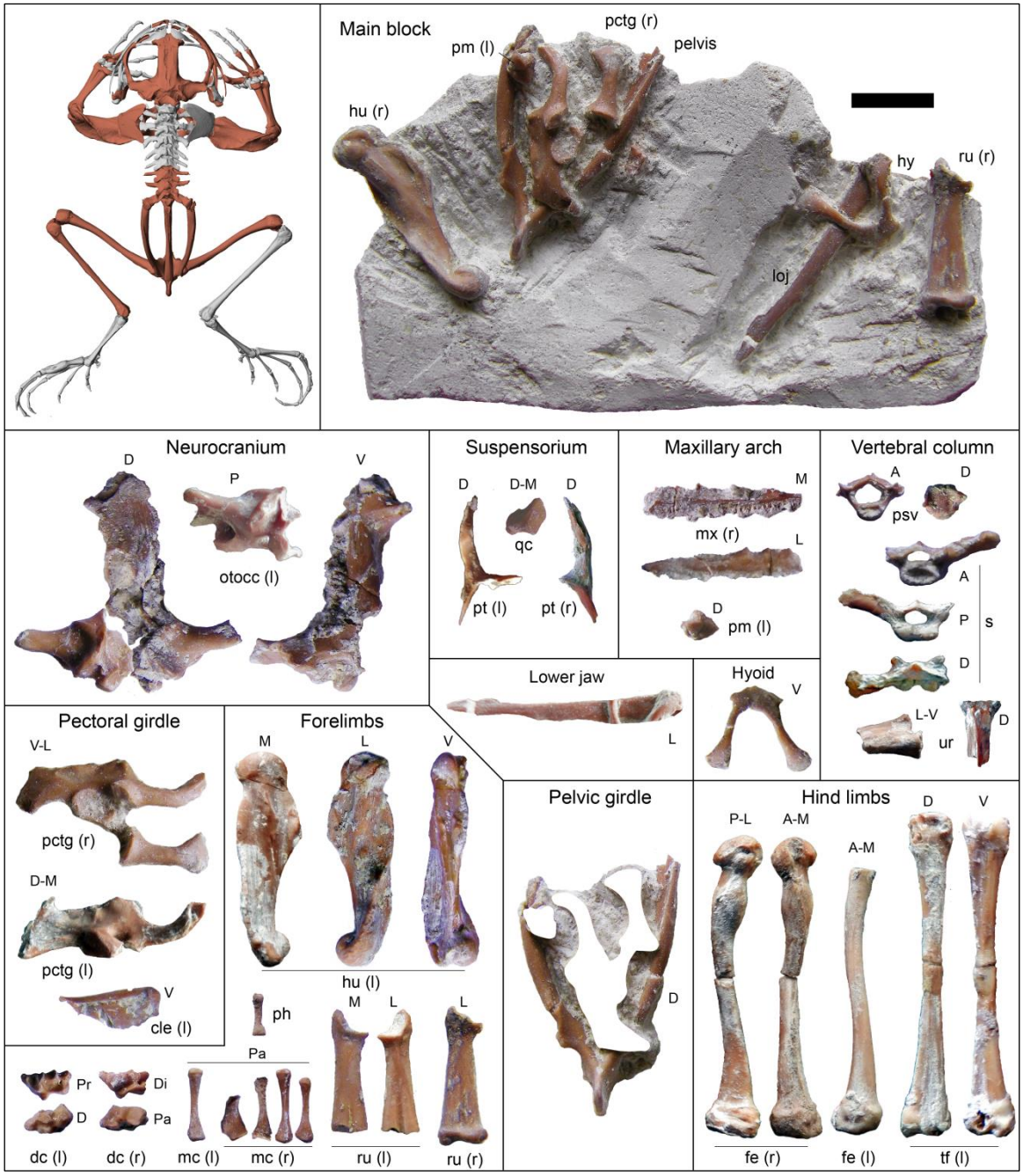

FIG. S1. *Telmatobius achachila* sp. nov., holotype (MNHN-Bol-V 012795). Photographs of the type block (top right) and mechanically isolated fossils representing a single adult male individual and restoration of the skeleton in dorsal view (top left; based on T. thompsoni UF-H 39734, not to scale) with the preserved parts coloured. The left premaxilla, hyoid, right lower jaw, right pectoral girdle, right radio-ulna, and pelvic girdle from the main block are depicted also isolated, but remain in the block. *Abbreviations*: (l), left; (r), right; A, anterior view; cle, cleithrum; D, dorsal view; dc, Distal Carpal 5-4-3; Di, distal view; fe, femur; hu, humerus; hy, hyoid; L, lateral view; loj, lower jaw; M, medial view; mc, metacarpal; mx, maxilla; otocc, otoccipital; P, posterior view; Pa, palmar view; pctg, pectoral girdle; ph, phallanx; pm, premaxilla; Pr, proximal view; psv, presacral vertebra; pt, pterygoid; qc, quadrate-quadratojugal complex; ru, radio-ulna; s, sacrum; tf, tibiofibula; ur, urostyle; V, ventral view. Scale bar represents 1 cm.

Appendix S3. Substrate preference, main habitat, and mean elevation above the sea level (ASL) of 44 *Telmatobius* species based on the IUCN Red List of Threatened Species (www.iucnredlist.org).

Telmatobius	**Substrate preference**	**Habitat**	**Elevation ASL (m)**
achachila	Aquatic*	Forests*	1600*
arequipensis	Semi-aquatic	Shrubland/grassland	3200
atacamensis	Aquatic	Highland wetlands	3800
atahualpai	Semi-aquatic	Forests	3050
bolivianus	Aquatic	Forests	2550
brachydactylus	Semi-aquatic	Shrubland/grassland	4300
brevipes	Semi-aquatic	Forests	3150
carrillae	Semi-aquatic	Shrubland/grassland	4240
ceiorum	Semi-aquatic	Forests	1750
contrerasi	Aquatic	Highland wetlands	3030
culeus	Aquatic	Highland wetlands	3810
degener	Semi-aquatic	Shrubland/grassland	3920
halli (dankoi)	Aquatic	Highland wetlands	2700
halli (vilamensis)	Aquatic	Highland wetlands	2700
hauthali	Aquatic	Highland wetlands	3960
hintoni	Aquatic	Highland wetlands	3550
huayra	Aquatic	Highland wetlands	4200
hypselocephalus	Aquatic	Shrubland/grassland	3550
ignavus	Semi-aquatic	Forests	2460
jelskii	Semi-aquatic	Shrubland/grassland	3542.5
laticeps	Aquatic	Shrubland/grassland	3050
latirostris	Semi-aquatic	Forests	2620
macrostomus	Aquatic	Highland wetlands	3750
marmoratus	Aquatic	Highland wetlands	3522
mayoloi	Aquatic	Highland wetlands	3832.5
necopinus	Semi-aquatic	Forests	2050
niger	Terrestrial	Forests	3234.5
oxycephalus	Semi-aquatic	Forests	2190
peruvianus	Semi-aquatic	Shrubland/grassland	3140
pinguiculus	Aquatic	Shrubland/grassland	3700
pisanoi	Aquatic	Shrubland/grassland	2750
platycephalus	Aquatic	Shrubland/grassland	3675
rimac	Semi-aquatic	Shrubland/grassland	3000
rubigo	Aquatic	Shrubland/grassland	3650
schreiteri	Aquatic	Highland wetlands	1925
scrocchii	Aquatic	Highland wetlands	2250
sibiricus	Terrestrial	Forests	2450
simonsi	Aquatic	Forests	1900
stephani	Aquatic	Forests	2250
thompsoni	Semi-aquatic	Forests	3290
timens	Terrestrial	Forests	3550
truebae	Semi-aquatic	Forests	2875
verrucosus	Semi-aquatic	Forests	3200
yuracare	Aquatic	Forests	3000

*Inferred for the fossil species. See text for details.

Appendix S4. Phylogenetic trees.

Strict consensuses obtained in the phylogenetic analyses of datasets B17 and GT21. See material and method for details. In GT21, the *Telmatobius bolivianus* species group is represented by *T. oxycephalus*, *T. hauthali*, and *T. scrocchii*. *Abbreviations*: B17, derived from that of Barrionuevo (2017); CI, Consistency Index; GT21, derived from that of Gómez & Turazzini (2021); MPTs, most parsimonious trees; RI, Retention Index.

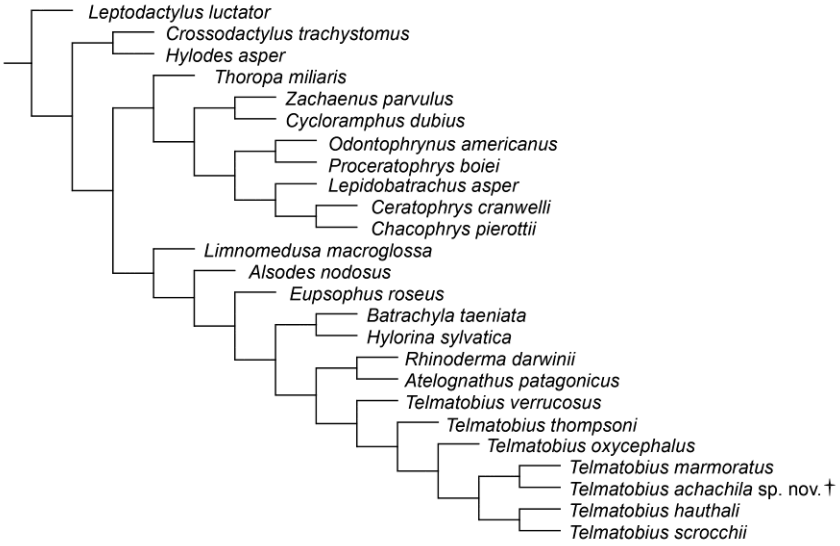

FIG. S2. Topology of single MPT (671–681 steps; CI = 0.476–0.483; RI = 0.569–0.581) obtained with dataset GT21 under implied weights with k = 5–9.

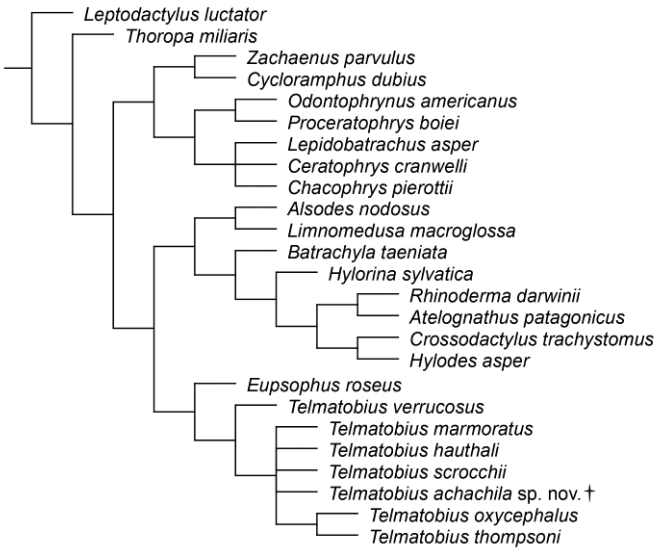

FIG. S3. Topology of the strict consensus of six MPTs (671 steps; CI = 0.483; RI = 0.581) obtained with dataset GT21 under equal weights and multistate characters unordered.

FIG. S4. Topology of the strict consensus of 144 MPTs (327.079 steps; CI = 0.363; RI = 0.721) obtained with dataset B17 under equal weights and multistate characters ordered.

FIG. S5. Topology of the strict consensus of 576 MPTs (320.108 steps; CI = 0.371; RI = 0.728) obtained with dataset B17 under equal weights and multistate characters unordered.

FIG. S6. Topology of the strict consensus of 232 MPTs (329.332–330.332 steps; CI = 0.359–360; RI = 0.717–0.718) obtained with dataset B17 under implied weights with k = 5–7 and multistate characters ordered.

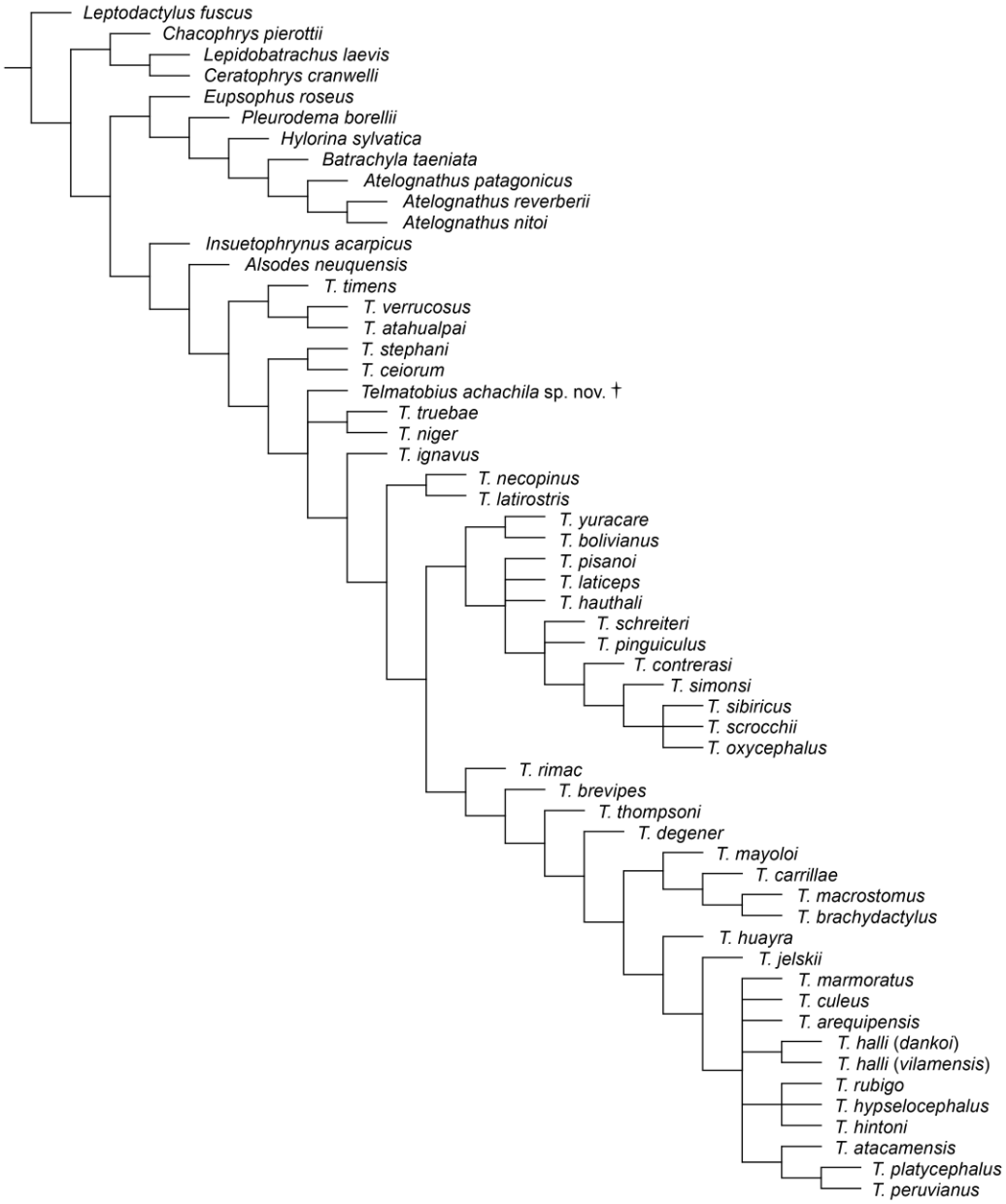

FIG. S7. Topology of the strict consensus of four MPTs (322.430 steps; CI = 0.368; RI = 0.725) obtained with dataset B17 under implied weights with k = 5–7 and multistate characters unordered.

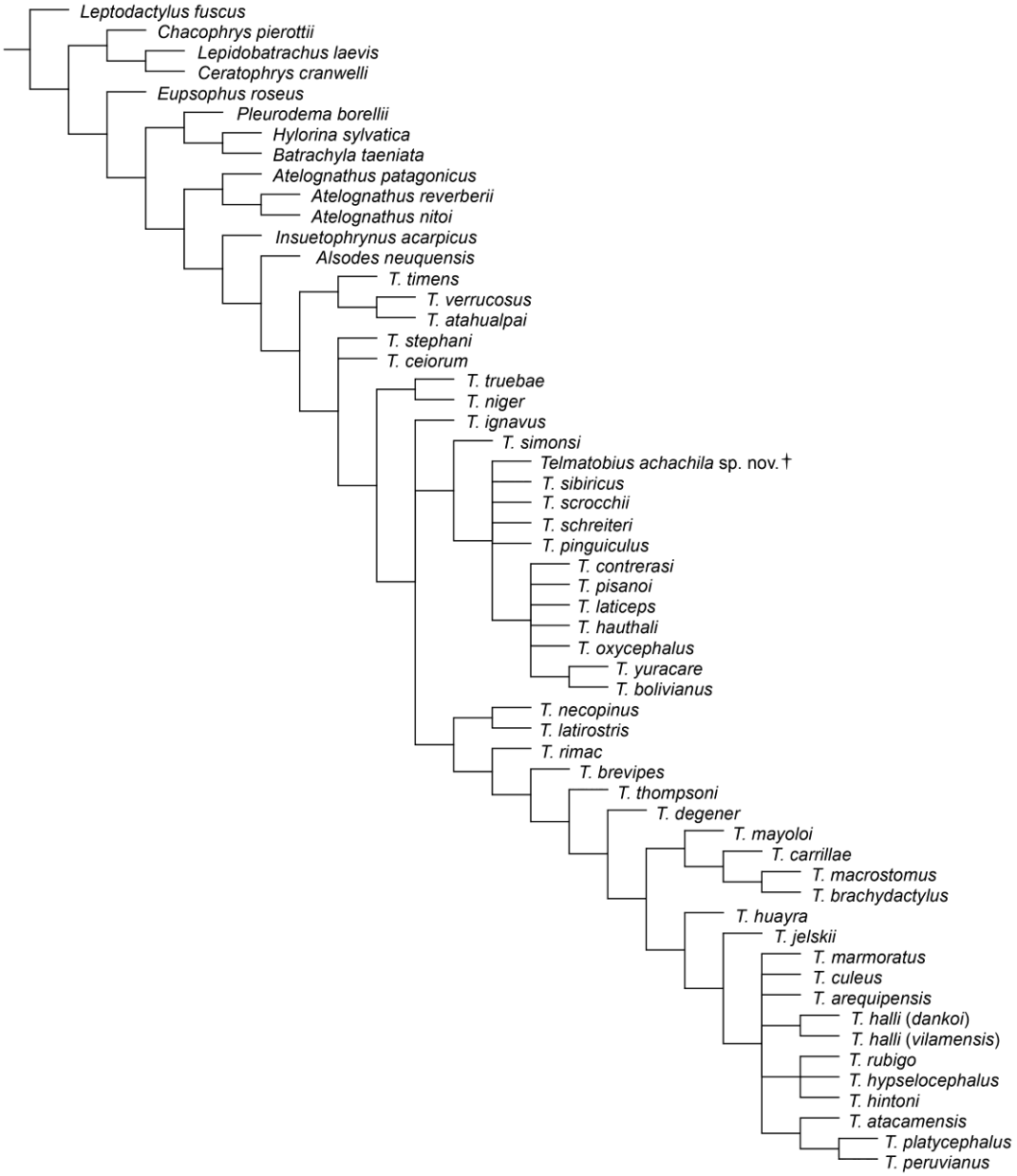

FIG. S8. Topology of the strict consensus of 100 MPTs (328.332 steps; CI = 0.361; RI = 0.720) obtained with dataset B17 under implied weights with k = 8–9 and multistate characters ordered.

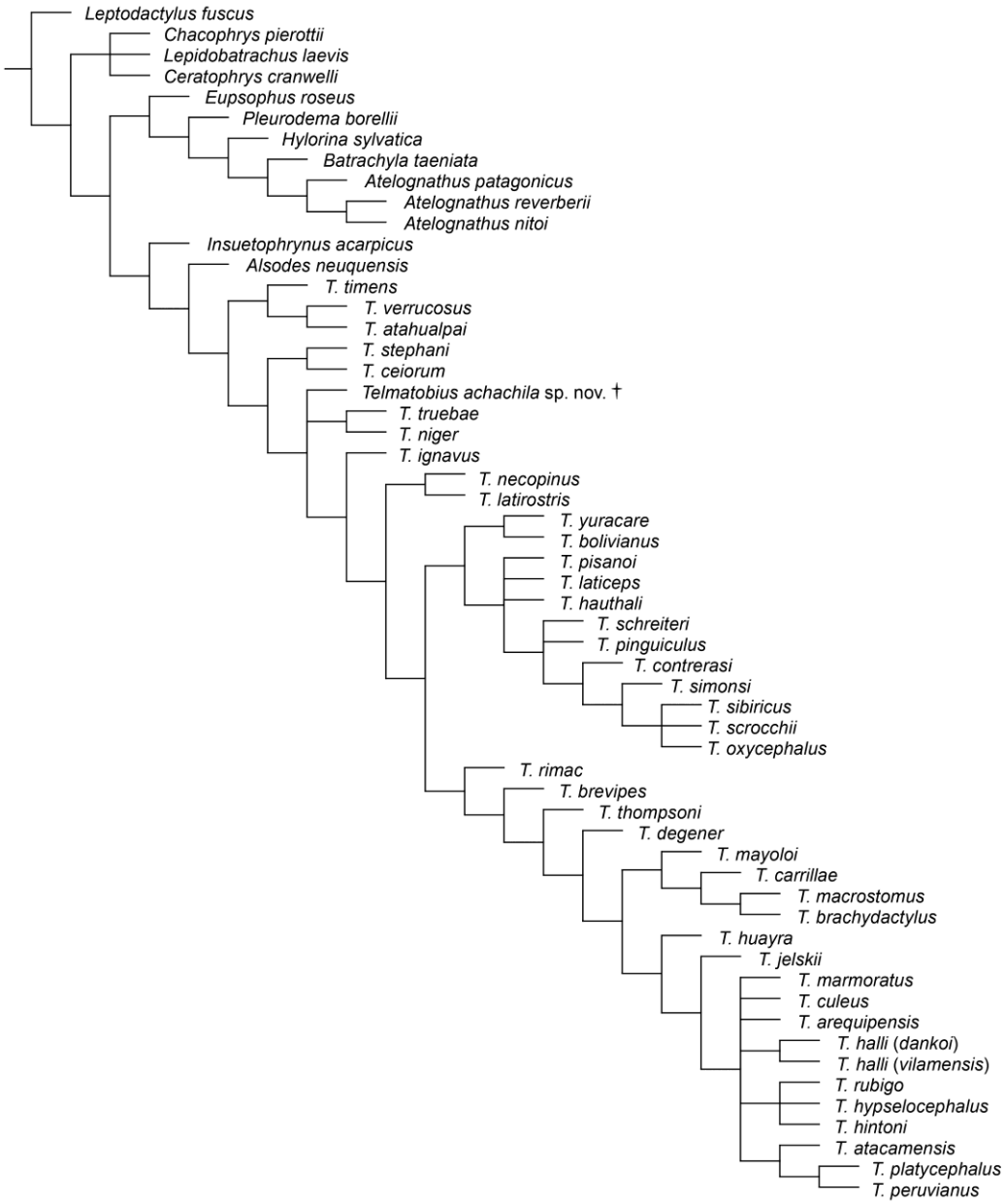

FIG. S9. Topology of the strict consensus of eight MPTs (322.430 steps; CI = 0.368; RI = 0.725) obtained with dataset B17 under implied weights with *k* = 8–9 and multistate characters unordered.

REFERENCES

AGUILAR, C., CATENAZZI, A., VENEGAS, P. J. and SIU-TING, K. 2012. Morphological variation of *Telmatobius atahualpai* (Anura: Telmatobiidae) with comments on its phylogenetic relationships and synapomorphies for the genus. *Phyllomedusa*, **11**, 37–49.

BARRIONUEVO, J. S. 2013. Osteology and postmetamorphic development of *Telmatobius oxycephalus* (Anura: Telmatobiidae) with an analysis of skeletal variation in the genus. *Journal of Morphology*, **274**, 73–96.

BARRIONUEVO, J. S. 2016. Independent evolution of suction feeding in Neobatrachia: feeding mechanisms in two species of *Telmatobius* (Anura: Telmatobiidae). *Anatomical Record*, **299**, 181–196.

BARRIONUEVO, J. S. 2017. Frogs at the summits: phylogeny of the Andean frogs of the genus *Telmatobius* (Anura, Telmatobiidae) based on phenotypic characters. *Cladistics*, **33**, 41–68.

BARRIONUEVO, J. S. 2018. Growth and cranial development in the Andean frogs of the genus *Telmatobius* (Anura: Telmatobiidae): exploring the relation of heterochrony and skeletal diversity. *Journal of Morphology*, **279**, 1269–1281.

BARRIONUEVO, J. S. and BALDO, D. 2009. Description of the tadpoles of *Telmatobius platycephalus* and *Telmatobius pinguiculus* from montane regions of Argentina. *Herpetological Journal*, **19**, 21–27.

BENAVIDES, E., ORTIZ, J. C. and SITES, J. W. J. 2002. Species boundaries among the *Telmatobius* (Anura: Leptodactylidae) of the Lake Titicaca Basin: allozyme and morphological evidence. *Herpetologica*, **58**, 31–55.

CUEVAS, C. C. and FORMAS, J. R. 2002. *Telmatobius philippii*, una nueva especie de rana acuática de Ollagüe, norte de Chile (Leptodactylidae). *Revista Chilena de Historia Natural*, **75**, 245–258.

DE LA RIVA, I. 1994. A new aquatic frog of the genus *Telmatobius* (Anura: Leptodactylidae) from Bolivian cloud forests. *Herpetologica*, **50**, 38–45.

DE LA RIVA, I. and HARVEY, M. 2003. A new species of *Telmatobius* from Bolivia and a redescription of *T. simonsi* Parker, 1940 (Amphibia: Anura: Leptodactylidae). *Herpetologica*, **59**, 127–142.

DE LA RIVA, I., TRUEB, L. and DUELLMAN, W. E. 2012. A new species of *Telmatobius* (Anura: Telmatobiidae) from Montane forest Southern Peru, with a review of osteological features of the genus. *South American Journal of Herpetology*, **7**, 91–109.

DUELLMAN, W. E. and CAMPBELL, J. A. 1992. Hylid frogs of the genus *Plectrohyla*: systematics and phylogenetic relationships. *Miscellaneous publications Museum of Zoology, University of Michigan*, **181**, 1–32.

DUELLMAN, W. E., DE LA RIVA, I. and WILD, E. R. 1997. Frogs of the *Hyla armata* and *Hyla pulchella* Groups in the Andes of South America, with definitions and analyses of phylogenetic relationships of andean groups of *Hyla*. *Scientific Papers*, **3**, 1–41.

FAIVOVICH, J., LUGLI, L., LOURENÇO, A. C. C. and HADDAD, C. F. 2009. A new species of the *Bokermannohyla martinsi* group from central Bahia, Brazil with comments on *Bokermannohyla* (Anura: Hylidae). *Herpetologica*, **65**, 303–310.

FORMAS, J. R., BENAVIDES, E., and CUEVAS, C. 2003. A new species of *Telmatobius* (Anura: Leptodactylidae) from Río Vilama, northern Chile, and the redescription of *T. halli* Noble. *Herpetologica*, **59**, 253–270.

FORMAS, J. R., CUEVAS, C. and NUNEZ, J. J. 2006. A new species of *Telmatobius* (Anura, Leptodactylidae) from Northern Chile. *Herpetologica*, **62**, 173–183.

GÓMEZ, R. O. and TURAZZINI, G. F. 2021a. The fossil record and phylogeny of South American horned frogs (Anura, Ceratophryidae). *Journal of Systematic Palaeontology*, **19**, 91–130.

IUCN SSC Amphibian Specialist Group. 2020. *Telmatobius culeus.* Errata version published in 2020 (03/06/2023). The IUCN Red List of Threatened Species 2020: e.T57334A178948447. https://dx.doi.org/10.2305/IUCN.UK.2020-2.RLTS.T57334A178948447.en

LAVILLA, E. O. and ERGUETA SANDOVAL, P. 1995. Una nueva especie de *Telmatobius* (Anura: Leptodactylidae) del Sudoeste de Bolivia. *Ecología en Bolivia*, **24**, 91–101.

LAVILLA, E. O. and ERGUETA SANDOVAL, P. 1999. A new Bolivian species of the genus *Telmatobius* (Anura: Leptodactylidae) with a humeral spine. *Amphibia-Reptilia*, **20**, 55-64.

TRUEB, L. 1979. Leptodactylid frogs of the genus *Telmatobius* in Ecuador with the description of a new species. *Copeia*, **1979**, 714–733.

WIENS, J. J. 1993. Systematics of the leptodactylid frog genus *Telmatobius* in the Andes of northern Peru. *Occasional Papers of the Museum of Natural History, University of Kansas*, **162**, 1–76.

Family	Genus	Species	Source	Specimen number	DOI
Telmatobiidae	Telmatobius	atahualpai	Aguilar et al. 2012	-	-
Telmatobiidae	Telmatobius	bolivianus	Lavilla & Ergueta Sandoval 19	-	-
Telmatobiidae	Telmatobius	brevipes	MorphoSource	UF:herp:39760	https://doi.org/10.17602/M2/M386402
Telmatobiidae	Telmatobius	carrillae	MorphoSource	UF:herp:39717	https://doi.org/10.17602/M2/M159469
Telmatobiidae	Telmatobius	chusimensis	Formas et al. 2006	-	-
Telmatobiidae	Telmatobius	cirrhacelis	Trueb 1979	-	-
Telmatobiidae	Telmatobius	culeus	MorphoSource	USNM:Amphibians & Reptiles:281587	https://doi.org/10.17602/M2/M423141
Telmatobiidae	Telmatobius	degener	MorphoSource	UF:herp:39736	https://doi.org/10.17602/M2/M99912
Telmatobiidae	Telmatobius	halli (dankoi/vilam	Formas et al. 2003	-	-
Telmatobiidae	Telmatobius	hauthali	Dry skeleton	FCEN 320, FML 3315	-
Telmatobiidae	Telmatobius	huayra	Lavilla & Ergueta Sandoval 19	-	-
Telmatobiidae	Telmatobius	ignavus	Wiens 1993	-	-
Telmatobiidae	Telmatobius	laticeps	MorphoSource	CAS:sua:11270	https://doi.org/10.17602/M2/M49875
Telmatobiidae	Telmatobius	latirostris	Wiens 1993	-	-
Telmatobiidae	Telmatobius	macrostomus	Dry skeleton	FCEN 1208-1	-
Telmatobiidae	Telmatobius	marmoratus	MorphoSource	CAS:herp:152217	https://doi.org/10.17602/M2/M49889
Telmatobiidae	Telmatobius	marmoratus	Dry skeleton	KU:kuh 164079, 164080	-
Telmatobiidae	Telmatobius	mendelsoni	De la Riva et al. 2012	-	-
Telmatobiidae	Telmatobius	necopinus	Wiens 1993	-	-
Telmatobiidae	Telmatobius	niger	Trueb 1979	-	-
Telmatobiidae	Telmatobius	oxycephalus	Cleared & stained specimen	FML 2867-II	-
Telmatobiidae	Telmatobius	oxycephalus	Barrionuevo 2013, 2016, 2018	-	-
Telmatobiidae	Telmatobius	philippii	Cuevas & Formas 2002	-	-
Telmatobiidae	Telmatobius	rubigo	Barrionuevo & Baldo 2009; Ba	-	-
Telmatobiidae	Telmatobius	schreiteri	Dry skeleton	FML 541	-
Telmatobiidae	Telmatobius	scrocchii	Dry skeleton	FML 1515	-
Telmatobiidae	Telmatobius	sibiricus	De la Riva & Harvey 2003	-	-
Telmatobiidae	Telmatobius	thompsoni	MorphoSource	UF:herp:39734	https://doi.org/10.17602/M2/M20345
Telmatobiidae	Telmatobius	thompsoni	Wiens 1993	-	-
Telmatobiidae	Telmatobius	truebae	Wiens 1993	-	-
Telmatobiidae	Telmatobius	vellardi	Trueb 1979	-	-
Telmatobiidae	Telmatobius	verrucosus	Cleared & stained specimen	CBF 5372	-
Telmatobiidae	Telmatobius	yuracare	De la Riva 1994	-	-
Alsodidae	Alsodes	nodosus	MorphoSource	cm:herps:68395	https://doi.org/10.17602/M2/M20871
Alsodidae	Alsodes	nodosus	Dry skeleton	FCEN 722	-
Alsodidae	Eupsophus	roseus	MorphoSource	cm:herps:63926	https://doi.org/10.17602/M2/M21082
Alsodidae	Eupsophus	roseus	Dry skeleton	AMNH:A-22140	-
Alsodidae	Limnomedusa	macroglossa	Dry skeleton	CFA-An 138, 192	-
Alsodidae	Limnomedusa	macroglossa	MorphoSource	cm:herps:55388	https://doi.org/10.17602/M2/M116724
Batrachylidae	Atelognathus	patagonicus	MorphoSource	cas:herp:141967	https://doi.org/10.17602/M2/M21953
Batrachylidae	Batrachyla	taeniata	MorphoSource	cas:herp:85253	https://doi.org/10.17602/M2/M21960
Batrachylidae	Hylorina	sylvatica	Dry skeleton	FCEN 304	-
Batrachylidae	Hylorina	sylvatica	MorphoSource	cas:herp:141996	https://doi.org/10.17602/M2/M22182
Bufonidae	Rhinella	spinulosa	Dry skeleton and cleared & st	MACN-He 45407–45409, 45413	-
Calyptocephalel	Calyptocephalel	gayi	Dry skeleton	FCEN 1433	-
Calyptocephalel	Calyptocephalel	gayi	Dry skeleton	MACN-He 45741–45747	-
Calyptocephalel	Calyptocephalel	gayi	MorphoSource	cas:herp:10082	https://doi.org/10.17602/M2/M24452
Calyptocephalel	Telmatobufo	bullocki (as venusti	MorphoSource	ku:kuh:161438	https://doi.org/10.17602/M2/M42671
Calyptocephalel	Telmatobufo	bullocki (as venusti	Dry skeleton	ku:kuh:161439	-
Ceratophryidae	Ceratophrys	cranwelli	Dry skeleton	CFA-An-73, 104, FCEN 665(2–4), 1015(	-
Ceratophryidae	Ceratophrys	cranwelli	MorphoSource	mcz:herp:A-35360	https://doi.org/10.17602/M2/M70811
Ceratophryidae	Chacophrys	pierottii	Dry skeleton and cleared & st	MACN-He 47403–47404	-
Ceratophryidae	Chacophrys	pierottii	MorphoSource	ku:kuh:191932	https://doi.org/10.17602/M2/M37697
Ceratophryidae	Lepidobatrachu	asper	Dry skeleton	FCEN 261 (1), 306, 439 (1, 2), 630 (1–3	-
Ceratophryidae	Lepidobatrachu	asper	MorphoSource	mcz:herp:A-32777	https://doi.org/10.17602/M2/M68634
Cycloramphidae	Cycloramphus	dubius	Dry skeleton	FCEN 758	-
Cycloramphidae	Cycloramphus (:	parvulus	MorphoSource	cas:sua:11907	https://doi.org/10.17602/M2/M23008
Cycloramphidae	Thoropa	miliaris	Dry skeleton	FCEN 595	-
Cycloramphidae	Thoropa	miliaris	MorphoSource	cm:herps:68357	https://doi.org/10.17602/M2/M24444
Hemiphractidae	Gastrotheca	peruana	MorphoSource	uf:herp:65801	https://doi.org/10.17602/M2/M55543
Hylidae	Boana	heilprini	MorphoSource	uf:herp:57613	https://doi.org/10.17602/M2/M162134
Hylidae	Boana	pulchella	Dry skeleton	CFA-An-273, 276	-
Hylidae	Boana	riojana	Cleared & stained specimen	IBIGEO-A (formerly MCN) 937	-
Hylidae	Bokermannohyl	circumdata	MorphoSource	ku:kuh:91987	https://doi.org/10.17602/M2/M162136
Hylidae	Bokermannohyl	langei	Faivovich et al. 2009	-	-
Hylidae	Hyloscirtus	armatus	Duellman et al. 1997	-	-
Hylidae	Phyllomedusa	hypochondrialis	MorphoSource	amnh:A-166281	https://doi.org/10.17602/M2/M165653
Hylidae	Phyllomedusa	sauvagii	Dry skeleton	FCEN 305	-
Hylidae	Plectrohyla	-	Duellman & Campbell 1992	-	-
Hylidae	Pseudis	paradoxa	MorphoSource	uf:herp:71527	https://doi.org/10.17602/M2/M163224
Hylidae	Pseudis	paradoxa	Dry skeleton	AMNH:A-71427; KU:kuh:167676	-
Hylodidae	Crossodactylus	trachystomus	MorphoSource	cm:herps:2662	https://doi.org/10.17602/M2/M24014
Hylodidae	Hylodes	asper	Dry skeleton	FCEN 762	-
Hylodidae	Hylodes	asper	MorphoSource	cm:herps:45975	https://doi.org/10.17602/M2/M34358
Leptodactylidae	Leptodactylus	fuscus	Dry skeleton	FCEN 711, 1704	-
Leptodactylidae	Leptodactylus	luctator (ex latrans	Dry skeleton	CFA-An 128, 131, 185; FCEN 283, 1931	-
Leptodactylidae	Leptodactylus	pentadactylus	MorphoSource	uf:herp:103788	https://doi.org/10.17602/M2/M50004
Leptodactylidae	Pleurodema	cinereum	Dry skeleton	FCEN 93	-
Leptodactylidae	Pleurodema	nebulosum	MorphoSource	cas:sua:15635	https://doi.org/10.17602/M2/M46050
Microhylidae	Hamptophryne	boliviana	MorphoSource	amnh:herpetology:a-115764	https://doi.org/10.17602/M2/M154612
Odontophrynid	Odontophrynus	americanus	Dry skeleton	CFA-An 129, 135; FCEN 1096, 1285	-
Odontophrynid	Odontophrynus	americanus	MorphoSource	cm:herps:147828	https://doi.org/10.17602/M2/M25346
Odontophrynid	Proceratophrys	boiei	Dry skeleton	FCEN 699	-

Family	Genus	Species	Source	Specimen number	DOI
Odontophrynid	Proceratophrys	boiei	MorphoSource	cm:herps:45986	https://doi.org/10.17602/M2/M29141
Pipidae	Pipa	aspera	MorphoSource	mvz:amphibian and reptile specimens:	https://doi.org/10.17602/M2/M165891
Pipidae	Pipa	carvalhoi	Dry skeleton	MACN-He 42606–42608	-
Pipidae	Pipa	carvalhoi	Cleared & stained specimen	MACN-He 42609–42610	
Pipidae	Pipa	carvalhoi	MorphoSource	mcz:herp:a-25737	http://mczbase.mcz.harvard.edu/guid/MCZ:Herp:A-25737
Pipidae	Pipa	parva	MorphoSource	uf:herp:37924	https://doi.org/10.17602/M2/M12424
Pipidae	Pipa	pipa	Dry skeleton	FCEN 1434; MACN-He 42612, 42613	-
Pipidae	Pipa	pipa	MorphoSource	usnm:herp:85032	https://doi.org/10.17602/M2/M405740
Pipidae	Pipa	snethlageae	Dry skeleton	MACN-HE 42611	-
Pipidae	Pipa	snethlageae	MorphoSource	mcz:herp:a-17734	https://doi.org/10.17602/M2/M66254
Pipidae	Xenopus	borealis	MorphoSource	cas:herp:152778	https://doi.org/10.17602/M2/M58062
Rhinodermatida	Rhinoderma	darwinii	MorphoSource	uf:herp:62022	https://doi.org/10.17602/M2/M25059
Strabomantidae	Pristimantis	duellmani	MorphoSource	ku:kuh:179333	https://doi.org/10.17602/M2/M61984